FINAL PUBLISHABLE JRP REPORT

JRP-Contract number	HLT06
JRP short name	MRI Safety
JRP full title	Metrology for next-generation safety standards and equipment in MRI
Version numbers of latest contracted Annex Ia and Annex Ib against which the assessment will be made	Annex Ia: V1.1 Annex Ib: V1.0
Period covered (dates)	From 01 April 2012 To 31 March 2015
JRP-Coordinator	
Name, title, organisation	Bernd Ittermann, PhD, PTB
Tel:	+49 30 3481 7318
Email:	bernd.ittermann@ptb.de
JRP website address	www.ptb.de/emrp/mri.html
Other JRP-Partners	
Short name, country	INRIM, Italy VSL, The Netherlands
REG-Researcher (associated Home Organisation)	
Researcher name, title	Jeffrey Hand, Prof.
(Home organisation Short name, country)	KCL, UK
	Start date: 1 June 2012
	Duration: 34 months

EMRP
European Metrology Research Programme
Programme of EURAMET

The EMRP is jointly funded by the EMRP participating countries within EURAMET and the European Union

TABLE OF CONTENTS

1 Executive Summary

This research project has contributed to the safer application of magnetic resonance imaging (MRI). A new patient safety concept developed in this project will help manufacturers to speed up innovation cycles and will allow the safe scanning of previously excluded patient groups. In addition, a foundation has been laid to bring a ground-breaking new technology in cancer treatment, MRI guided radiotherapy, to the patient.

The Problem
The health and safety of European citizens and the effectiveness of medical procedures needs to be improved. Each year, about 23 million EU citizens undergo an MRI scan during which their body is exposed to powerful and potentially hazardous radiofrequency (RF) pulses. Tissue heating is an established health risk for patients and is caused by absorbed (RF) power (measured by the Specific Absorption Rate (SAR) in watts per kilogram). In order to ensure the body is not exposed to unsafe levels the distribution of the RF electromagnetic fields inside the body has to be monitored. The traditional approach to assess MRI safety had limitations and became a barrier for innovation as it is not applicable to emerging MRI technologies such as ultrahigh field strengths (e.g. 7 T) or parallel RF transmitters (pTx) and is not capable of dealing with patients carrying a metallic medical implant. A new safety concept based on numerical simulations to compute the distribution of RF electromagnetic fields inside the human body is in principle well suited to solve both problems. However, additional work needed to be carried out to validate the simulation results, to quantify their uncertainty, and to establish whether the concept can deal with metallic implants and emerging technologies. This would strengthen the market position of the European Medical Technology industry. The European directive 2004/40/EC on the minimum health and safety requirements regarding the exposure of workers to the risks arising from electromagnetic fields has raised concerns that the directive might effectively ban MRI as employees might no longer be allowed to approach an MRI scanner and therefore work needed to be done to quantify these risks to provide advice for EU decision makers and strengthen the citizens' confidence in their decisions. Furthermore, MRI is an ideal candidate to be used in image guided radiotherapy for cancer treatment however it poses the new problem of how to provide reliable and traceable data on exposure levels (photon dosimetry) within the electromagnetically harsh environment of an MRI scanner.

The Solution
The overall aim of the project was to enhance the safety of MRI for patients and staff while simultaneously eliminating *unnecessarily* restrictive exposure limits, thus improving the diagnostic value and efficiency of MRI. By providing a rigid risk assessment for emerging technologies such as ultrahigh magnetic fields, parallel transmission or MRI guided radiotherapy, the project intended to support a faster market introduction of new developments from European manufacturers.

Impact
It will take years before the full impact of the MRI Safety project is achieved and can be assessed. Nevertheless, there is some 'early impact' which can already be reported. Representatives from Elekta, leading European manufacturer of radiotherapy equipment, confirmed in March 2013 that "*... The EMRP project HLT06 contributes exact and reliable radiation dosimetry to this endeavor, an indispensable precondition before any patient can be treated. Thanks to EMRP results manufacturers Elekta were in the position to make the next step...*" i.e. bring the innovative radiotherapy system to the market. Project partners from Turin developed a new formulation to calculate motion induced electromagnetic fields in the human body. Australian colleagues recognized the value of that approach and a fruitful cooperation emerged, resulting in three journal papers and two conference proceedings, so far. Scientists from the Berlin Ultrahigh Field Facility expressed interest in the methodology developed for metallic stents in MRI, resulting in one joint journal publication and three joint conference proceedings. Representatives from *Bundesamt für Strahlenschutz*, the German authority for radiation protection, and ICNIRP closely followed and interacted with the project from the start. Findings from the motion-induced field work affected statements in the guidelines. In its 2011 Research Agenda the World Health Organisation (WHO) stated a number of “high priority research needs" with respect to EMF dosimetry (i.e. including MRIs) for example to "*assess characteristic RF EMF emissions, exposure scenarios and corresponding exposure levels for new and emerging RF technologies and for changes in the use of established technologies: This work should address the latest developments in areas such as ... body imaging*". This request was successfully addressed as the project made a number of significant dosimetric contributions addressing the specific case of MRI. Methods were developed to assess characteristic MRI related RF

emissions in general and in particular for emerging technologies/changes in use of existing technologies like ultrahigh fields (e.g. 7T MRI scanners) and pTx.

2 Project context, rationale and objectives

2.1 Context

The research project HLT06 "MRI Safety" was designed to contribute to the following high-level goals:

- to improve the health and safety of European citizens;
- to improve the effectiveness and cost-effectiveness of medical procedures resulting in savings for the EU healthcare systems;
- to strengthen the market position of the European Medical Technology industry;
- to provide advice for EU decision makers by metrological underpinning of regulatory exposure limit values for patients, workers, or the general public;
- to strengthen the confidence of the European population in the rationality of EU regulatory decisions.

The specific field to pursue these high-level aims was Magnetic Resonance Imaging (MRI). MRI is an indispensable medical imaging modality with more than 23 million patient examinations per year in the EU and an excellent history of safe use. Nevertheless, it was effectively almost banned in Europe by the 2004/40/EC directive, whose revised version was published in 2011. The main reasons for this “near miss” were a lack of solid data and equally important a lack of communication between researchers from the MRI and metrology community and regulatory and advisory boards. This project aimed to address both issues by targeting a number of specific topics regarding patient and occupational safety in MRI.

The specific research goals of the "MRI Safety" project were largely inspired by explicit requests from a number of highly relevant organisations:

- the World Health Organisation (WHO) was concerned about the safety of patients, workers and the general public when exposed to EM fields and stated that metrologically sound dosimetry of such fields was missing;
- the International Society for Magnetic Resonance in Medicine (ISMRM), professional association of MRI researchers, requested more research in this area as it was concerned that regulatory decisions not based on reliable, quantitative data might put MRI as a diagnostic modality and as a thriving research field at risk;
- this view was also shared by the Deutsche Physikalische Gesellschaft (DPG), national professional association of physicists in Germany, who especially feared for the possible damage to the MRI and medical devices industry which are significant employers (not only) for physicists;
- the International Organization for Standardization (ISO) called for better and more reliable measurements to base future standards on MRI and implant safety upon;
- the International Commission on Non-Ionizing Radiation Protection (ICNIRP) is an international advisory board; they called for precise measurements as input data for the next set of guidelines they were preparing;
- the European Society of Radiology (ESR), professional association of medical researchers, was seriously concerned that in the absence of reliable scientific information premature regulatory decisions could be made which would effectively ban the future use of MRI in Europe.

Tissue heating by absorbed radio-frequency (RF) power (measured by the Specific Absorption Rate (SAR) in watts per kilogram) is an established health risk for patients. In the most advanced MRI scanners operating at “ultrahigh magnetic fields” (≥7 T) the RF wavelengths in water-like tissues come down to ~12 cm which is for the most relevant cases of head and torso smaller than the body part inside the RF coil. This brings the danger of temperature hot spots and emphasises the need for local SAR control. However, the local SAR distribution inside a human body can only be derived from numerical simulations. At the beginning of the project these could not be sufficiently trusted as no established means

existed to validate them. The research project aimed, therefore, to develop advanced modelling concepts for electromagnetic fields (EMF) inside phantoms and human computer models and to validate them by comparison to calibrated EMF measurements.

Physiological effects and potential hazards (especially) for clinical and maintenance staff moving through the strong magnetic stray fields of up to several tesla around MRI scanners were not sufficiently known. It was thus intended to assess the related physiological effects by combining dosimetric measurements and simulations.

Emerging technologies in MRI, such as ultrahigh fields or parallel transmission (pTx) technology, promise better image quality, shorter scan times, and better diagnostic value. With respect to SAR control, however, the transition from a conventional single-channel MRI scanner to a prototype 8-channel pTx system implies going from a 1-dimensional to a 15-dimensional parameter space. Established concepts to handle this challenge were just emerging at the beginning of the project and thus it was one major aim to further develop and most importantly to validate them.

The absence of ionizing radiation and the unmatched soft-tissue contrast of MRI make it the ideal candidate for the recent development of image guided radiotherapy of thoracic and abdominal tumours. These radiation targets exhibit large variation in position, size, and shape during the course of the radiotherapy treatment. This provoked the development of another emerging technology in MRI: despite the enormous technical difficulties to combine a linear accelerator (linac) for radiotherapy with an MRI scanner, a prototype system of an MRI-accelerator combination had been developed at the University Medical Centre Utrecht. The additional challenge of how to provide reliable and traceable photon dosimetry within the (electromagnetically) harsh environment of an MRI scanner was unmet, however. To close this dosimetric gap was another core goal of the reported research project.

An estimated 8 – 10 % of the European population are carrying medical implants. At present, this excludes them from receiving an MRI scan as no metrics exist to assess the specific safety risks related to these implants. For the subgroup of passive implants the research project aimed at an explorative investigation of implant associated risks with the ultimate goal of proposing such a metric, which is urgently requested by patients, physicians, manufacturers, and regulatory bodies. Due to given temporal and budgetary constraints it was clear from the beginning, however, that only some preliminary work in that direction would be achievable.

2.2 Objectives

MRI patients and staff were the targeted beneficiaries of the MRI Safety research project. The idea was, on the one hand, to enhance their safety while simultaneously allowing for the identification and adaptation of any *unnecessarily* restrictive exposure limits due to insufficient knowledge; thus leading to better image quality, improved diagnostic value and shorter scan times. By providing a rigid risk assessment for emerging technologies like ultrahigh magnetic fields, pTx or MRI-accelerator combinations, the project's goal was to help European manufacturers in streamlining their developmental targets and eliminating costly delays between product development and market introduction. To achieve this, an as direct as possible immediate impact on future safety standards, such as EN/IEC 60 601-2-33 and ISO DTS 10974, and other regulatory guidelines was aimed at.

The permanent close interaction of the research consortium with associated collaborators and stakeholders from the scientific community, leading manufacturers and advisory bodies was a crucial ingredient to ensure that the project results would make their impact outside of the field of metrology.

The joint research project on MRI Safety had been conceived to achieve the following scientific and technological objectives:

Objective 1: to develop a metrological concept and reference instrumentation in order to provide a set of traceable measurements of radio-frequency (RF) electromagnetic (EM) fields generated by MRI scanners, i.e. for frequencies in the range from 64 MHz to 300 MHz; to use these measurements to validate numerical modelling results;

Objective 2: to develop a mathematical modelling concept and use it to calculate RF electromagnetic field distributions and the related thermal effects inside the human body;

Objective 3: to assess the risk to human subjects from moving through the inhomogeneous static stray fields of MRI scanners; these fields are in the range of 100 mT up to 7 T and can induce slowly varying eddy currents (harmonic content of the order of 1 Hz) inside the human body;

Objective 4: to develop a validated measurement method suitable to assess the specific SAR hazards associated with emerging new MRI technologies such as parallel transmission (pTx) or ultrahigh magnetic fields (≥ 7 T);

Objective 5: to develop a dosimetry method for the newly emerging application of MRI in image guided radiotherapy, comprising a system for traceably measuring the absorbed dose to water for high energy photon beams in an MRI-accelerator combination, and to assess potential changes in relative biological effectiveness of accelerator photon beams due to the magnetic field.

Objective 6: to develop a concept to assess the risks due to the presence of passive, metallic, medical implants inside the patient's body during an MRI scan.

Objectives 1 and 2 define the foundations of the project by calling for the development of suitable experimental and computational methods respectively, as only the combination of both calibrated measurements and validated numerical simulations is capable to provide the desired results. Objective 3 requests the investigation of potential hazards particularly for clinical employees and service personnel when approaching the MRI scanner and moving through its strong magnetic stray field. Objectives 4 and 5 are both concerned with emerging technologies, exciting new developments in MRI which promise substantial added value for the patient (better diagnosis) and the health care system (reduced scan times and costs). Clarifying safety problems related to these new concepts as quickly as possible is key to reducing the delay time between the development of a first prototype and the arrival of a certified product in clinics. Objective O4 deals with the cases of parallel transmission and ultrahigh magnetic fields where safety hazards are intimately related to SAR control and the possibility of local SAR hotspots. Objective 5 asks to extend existing boundaries and to generate new patient benefits by supporting the fusion of MRI with therapeutic modalities. This objective is centred on dosimetry needs and understanding of biological effects in relation MRI-guided radiotherapy, i.e. the combination of an MRI scanner with treatment devices such as a linear accelerator. Finally, objective 6 addresses a problem which affects an ever-growing fraction of the EU population: how to ensure MRI safety for carriers of medical implants? Within the MRI Safety project the scope of this objective was restricted to the RF heating of implants as this is the most fundamental aspect affecting all metallic implants, both active and passive.

3 Research results

The following subsections summarize the major research results of the MRI Safety project. Five different research groups, from Berlin (Germany), Braunschweig (Germany), Delft (The Netherlands), London (United Kingdom), and Turin (Italy), all contributed their significant share to the results. At least two but more often three different groups were jointly working on each single objective and most groups were working on several objectives simultaneously. The following more detailed description of results is structured according to the list of objectives as defined above, i.e. subsections 3.1 to 3.6 correspond to objectives 1 to 6. Due to the inherent structure of the project as a closely interwoven network of partners *and* activities, in contrast, for instance, to a mere collection of relatively independent groups and tasks, the dividing lines between objectives could not always unambiguously be drawn. For a number of activities the assignment to one specific objective was somewhat arbitrary, therefore; they could as well have been reported in another subsection.

3.1 RF electromagnetic field measurements

Project partners from Berlin (PTB), Turin (INRIM) and London (KCL) joined their resources to work on the first project objective (O1). Due to that successful cooperation the objective could be fully achieved. Equipment and method developments described in this subsection were not only used to achieve objective O1 per se but were also one foundation for the later work on other objectives, like O2, O4, and O6.

3.1.1 *Versatile measurement infrastructure for RF safety assessment of state-of-the-art and future MRI systems*

One of the major goals of the project was the development of a metrologically sound infrastructure for the MRI environment to relate EMF simulations with measurements of diverse RF quantities. The metrological concept to assess the SAR hazards of MR imaging equipment is based on instrumentation providing traceable in situ measurements of RF electromagnetic fields and other RF related quantities in the MRI environment. These unique measurement methods developed by PTB are suitable for either state-of-the-art MR equipment at 1.5 T or 3 T or for emerging MRI technologies such as parallel transmission (pTx) or ultrahigh magnetic fields (≥ 7 T) with their specific associated RF related hazards. As a major result the established measurement infrastructure allows experimental validation of actual EMF field simulations of real MRI systems within reasonable uncertainty margins. Thus, the locally deposited RF power (peak spatial SAR averaged over 10g, psSAR10g) can be determined at a much higher level of confidence compared to contemporary safety standards.

The measurement infrastructure was developed with the aim of maximum independence from MR vendor specific solutions. Furthermore, it can be operated independently from the MR equipment allowing measurements in specific exposition scenarios which is important e.g. for safety assessments of metallic implants.

The developed MR safe measurement infrastructure is inert with respect to strong static magnetic fields and to switched magnetic field gradients. To avoid RF field distortions and RF interferences by metallic wires for all RF probes a fibre optical link was used for signal readout. Other measurement equipment is located outside the shielded MR scanner room. To account for the complex time structure of the pulsed transmitted RF signals all measurement devices operate in the time domain regime with full phase resolution capability.

The measurement infrastructure consists of five components:

i) Phantoms: One part of the measurement infrastructure for RF safety assessment are phantoms resembling the human body or parts of it. A body phantom is described in the ASTM standard F2182–11, however the height of only 9 cm used for implant testing seemed not suitable for the investigation of the EM fields in MRI. The JRP participants agreed in an early phase of the project to use a phantom with the outline described in the standard but a more realistic height of 15 cm filled with a Tween20 based phantom liquid developed by NPL. The body phantom of PTB was equipped with 5 removable tubes for EM field measurements in the interior and also with feedthroughs for wire type implants. As head phantom shell a cylinder with 20 cm diameter and 20 cm length equipped with 4 tubes was used. The dielectric properties of the phantom liquids were characterized by PTB using a coaxial probe. The liquid for the body phantom was also used in the laboratory phantom of INRIM for the assessment of the computational tools developed in the JRP.

The phantom liquids were originally developed for the use with cell phones to reproduce worse case exposure scenarios. Later in the project it was shown that their high conductivity caused untypical field distributions inside the phantom when used in MRI. This is no problem as far as the phantoms are used to validate simulations and to prove the methods developed. It would however pose a problem when the phantoms are used to assess implant safety. Since the high conductivity also causes unrealistic loading conditions in head coils it was decided later in the JRP to use a head phantom liquid with a conductivity customized to resemble the load of a human head. Together with the phantoms several tools for save body phantom handling (ca. 60 kg weight) and accurate phantom and sensor positioning were developed by PTB throughout the JRP.

ii) RF field generation: Usually, the RF chain of the MR scanner under investigation is used as RF field source. A state-of-the-art clinical MRI system comprises of a single channel multi-kilowatt pulsed RF amplifier directly connected to the birdcage type body coil used for spin excitation. To simplify the subsequent data analysis the MR scanner should run a pulse sequence with a rectangular RF pulse shape at a repetition rate of ≥ 1s. For RF field measurements in a parallel transmission MRI system pTx array coils are needed as field source and a more sophisticated sequence programming of the multi-channel RF signal generation chain of the system under investigation is required. To this end PTB implemented a versatile RF field measurement sequence on both its 3T and 7T MR systems with 8-channel parallel transmission capability. For bench measurements independent of the MR scanner, a separate pulsed RF generator together with broadband power amplifiers was used. Together with a 16-port Butler matrix

pTx coils can be driven with equal amplitudes and phase increments of multiples of 22.5 degrees. To measure the radiated RF power of pTx coils for 7T MRI systems PTB constructed a waveguide (l = 2.8 m, d = 0.6 m) mimicking the inner bore of a 7T MR magnet.

iii) MR compatible RF signal and field sensors: A set of eight directional couplers, nonmagnetic and specially customized for PTB, was used to measure the forward and reflected RF voltages at the feeding ports of pTx coils in either 3T or 7T MRI magnets. A time domain electro-optic *E*-field probe (OEFS-S1B, Seikoh-Giken) was used for *E*-field measurements inside and outside of the phantoms. The system consists of a three axis sensor head (d = 12 mm), an 11 m optical fibre link and a controller unit with RF output. The controller unit is always placed outside the RF shield of the scanner room. The optical link has to be fed through the filter plate of the MRI system. A homebuilt *H*-field pickup loop together with a time domain electro-optic transducer (OEFS-PH-0655, Seikoh-Giken) was used to measure B_1^+ and B_1^- fields using the same controller as the *E*-field probe. At the end of the project a commercial time domain *H*-field probe with optical read out (H-TDS, SPEAG) was available but due to its size this probe could only be used outside the project phantoms but not in the inner tubes. For measurements of RF currents at the protruding end of thin conductive wires a nonmagnetic current sensor based on a shielded Rogowski coil was developed and built by PTB. Signal read out was accomplished again with the time domain electro-optic transducer (OEFS-PH-0655, Seikoh-Giken).

For all MR safe field probes mounting assemblies were developed and built by PTB allowing proper positioning of the field probes inside and outside the phantoms, in the surrounding of a human subject and inside the calibration devices.

iv) Data acquisition: To handle the RF signals from the eight directional couplers to measure S-parameter matrices of pTx coils in situ a 16 × 1 switching matrix of high precision mechanical RF switches was built by PTB. The switching matrix itself is located inside the RF shield of the MR scanner room whereas the controller unit operates outside the shield. Suitable feedthroughs were implemented into the filter plate of the 3T and 7T MR scanner of PTB.

RF signals from field probes and directional couplers were digitized by a fast two channel transient recorder card suitable for RF signals up to 300 MHz. PTB developed a data acquisition system based on this card including flexible software for digital down conversion, filtering and subsequent data processing. Furthermore, the software is performing measurement control, i.e. synchronization with the MR sequence, trigger generation for the RF switch matrix and reference signal acquisition.

Fig. 3.1-1 *Collection of components of the versatile measurement infrastructure for RF safety assessment: data acquisition system (1), OEFS-controller (2), H-TDS-controller (3), RF source and broadband PA (4), MR-TEM cell (5), annular gantry for body coil (6), head phantom in 8-channel pTx coil (7), second head phantom (8), 16 port Butler matrix (9), calibration coil (10) for RF current sensor (11), body phantom (12), phantom liquids (13).*

v) Sensor calibration: An important feature of the metrological concept pursued within the JRP is the in-situ calibration of field probes. For calibration of time domain field sensors inside the MR scanner the nuclear spins of water protons are used as endogenous field probes where the clockwise rotating transversal field component B_1^+ is related to the gyromagnetic ratio γ_p of the proton. The technical details of this cell and of the calibration procedure will be described in a forthcoming publication.

3.1.2 Comprehensive characterization of 3T body coils

Knowledge of the EM fields in the body coils of MRI scanners is a precondition for the assessment of RF safety and of implant safety in particular. PTB thus explored how to generate a reliable coil model which predicts the fields not only qualitatively but quantitatively with limited a priori knowledge of that commercial coil. For home build coils where all details are available the feasibility of such models is undisputed. It was an open question, however, what kind of external measurements would be required to parameterize the coil model of a proprietary coil.

It was possible to obtain the geometry of the 16 rung body coil (CAD structure) of PTBs 3T VERIO scanner from the vendor (Siemens) together with the approximate values of the end ring capacitors. Furthermore the coil load and the positions of the trimmers used for matching, tuning and decoupling were known as well as details of the elliptic polarized driving mode used for body imaging.

The feeding ports of the body coil were not directly assessable to measurements, only the remote end of the feeding cables. The feeding voltage amplitudes and phases were measured both for circular and elliptic polarisation using a digital scope. Furthermore S-parameter and RE(Z) spectra where measured at the feeding cables as a function of loading conditions to determine the Q factor of the body coil.

For the EM simulations CST Microwave Studio (CST, Darmstadt, DE) was used. The values of the end ring capacitors as well as the trimmers used for matching, tuning and decoupling were refined using co-simulations (ADS, Agilent Technologies, Santa Clara, US). The feeding conditions measured were used to drive the coil and coil losses were introduced to reproduce the Q factors found experimentally.

The results of the EM simulations were first compared to B_1^+ maps of the body phantom in various positions in the body coil. The model was then optimized by minimizing the deviations to the measured field maps allowing for an additional phase shift caused by matching, tuning and decoupling.

The *E*-fields and *B*-fields measured with fibre optic time domain sensors inside and on top of the phantoms were in good agreement with the simulations. In particular the axial *E*-field profiles exhibit a lot of structure and even the multitude of minima and maxima of the minor field components were reproduced well. However, the *E*-field is quite sensitive to deviations of the real body phantom to the model of the body phantom pronouncing therefore these model deviations as a source of uncertainty. Therefore to evaluate the accuracy of the coil model measured B_1 field components turned out to be most useful.

Axial profiles on top of the phantom, e.g. as depicted in Fig. 3.1-2,were best suited to compare measured and simulated B_1 since the influence of positional errors is lower than for lateral profiles. Not every detail of the calculated B_1^+ and B_1^- distributions is in perfect agreement with the measurements but deviations were smaller than 10 % for B_1^+ values larger than 1 µT and also for the central z-profile of B_1^-. One measured B_1^- profile at the left hand side shows values about 17 % lower than the simulated ones in the central region of the coil. Such an asymmetry could arise from variation of properties of the lumped elements in the single rungs of the real coil.

To trace such deviations an annular gantry with wholes close to the rungs was build and used to measure phase and amplitude of the tangential B_1 component. This component is a measure of the current inside the rungs both for circular and elliptic polarization. The phases were in good agreement with values derived from FDTD simulations driving a generic coil model with the target currents and amplitudes. However after scaling the amplitudes the two topmost rungs were about 15 % higher than simulated while the others agreed well.

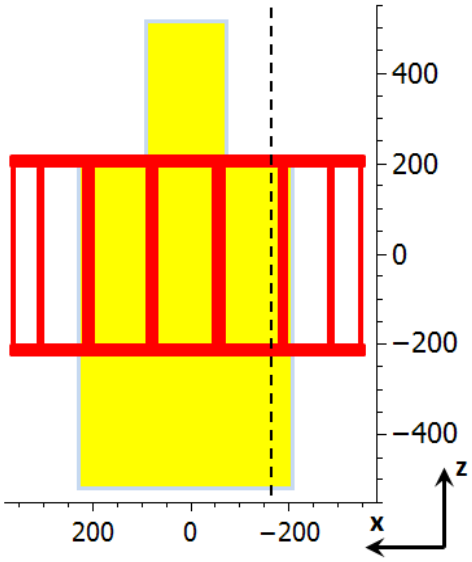

Fig. 3.1-2. *Body phantom filled with tissue simulating liquid within the 'body coil' RF transmitter of a clinical 3T scanner. The dashed line indicates one path on top of the phantom where sensor measurements were performed. Scales in mm.*

In summary, it is a considerable effort to iteratively refine the model of the body RF coil until satisfactory agreement with measured field profiles is obtained. The reason is that the detailed parameters of that proprietary coil are not disclosed by the vendor. Going through this optimization of the coil model is a necessary requirement, however, before the fields inside a human subject can be predicted with sufficient accuracy. Measurements inside humans are not feasible however profiles above the volunteer in a fixed vertical position can be recorded. A comparison with the B_1^+ profiles above the phantom clearly shows the sensitivity of the axial profiles to the object in the coil. Again, the B_1^+ fields show good agreement, however the measured values are about 17 % higher which can be attributed to different coil loading for the human voxel model DUKE and the actual volunteer. Consistently, agreement for the B_1^- profile at the left hand side is worst, suggesting the coil asymmetry is not perfectly reproduced in the model.

3.1.3 Summary: RF electromagnetic field measurements

- Reference instrumentation and methods for calibrated measurements of RF electromagnetic (*E*- and *B*-) fields were developed. This allowed the validity of simulation results to be checked with respect to the electromagnetic fields generated by the RF transmit coil of interest. The power associated with these fields is absorbed in the subject body; safety-wise this is the most critical part.
- The most widely used and hence most relevant RF transmit coil in an MRI scanner is the so-called body coil. It is an integral part of the hardware, not easily accessible and only imprecise, 'generic' models of these coils are available from the manufacturers. A detailed and validated coil model is a necessary requirement, however, for any quantitative simulation of the fields generated by this coil. A procedure was thus developed, allowing to test and iteratively refine the computer model of such a coil by comparing modelling predictions and measurements results at each step. The whole procedure was successfully applied to the body coil of a clinical scanner, demonstrating its effectiveness.
- Finally, the developed instrumentation was applied for a few reference measurements on different scanners and for different RF coils and the results were compared to simulations. The agreement was within about 10 % which is fully sufficient for the given purpose, demonstrating the validity of the concept.

3.2 RF electromagnetic field calculations

Currently a fundamental paradigm shift with respect to RF related safety in MRI is taking place as the traditional concept of controlling one single parameter, the total RF power delivered to the scanner's body coil, is known to be no longer adequate. It is universally accepted, that this concept needs to be

replaced by an assessment of the RF field distributions inside the human body. Such an assessment of all electric and magnetic components of the RF field plus derived quantities such as the specific absorption rate SAR (locally absorbed RF power per unit mass) can only be achieved by numerical modelling. It was thus the first task to investigate existing models, to develop new ones and compare the results. Equally important, however, is the second step: to develop concepts for a measurement based validation of these modelling results as without such a validation a modelling based approach to RF safety will not be implemented by the manufacturers of clinical scanners and all innovation in this field will be blocked.

This subsection describes the work related to achieving objective 2, which was the second core objective of the MRI Safety project. This role is emphasized by the fact that results of activities addressing objective 2 also entered into the work on four other objectives (1, 3, 4, and 6). Project partners from Italy (INRIM), UK (KCL) and Germany (PTB) were combining, extending and harmonizing their respective resources to address this task. This included a certain amount of intentional redundancy, e.g., solving the same problem at different sites using different software packages, for cross checking and mutual validation. Even more important were the concerted activities, however, e.g. when one group invested their capabilities and expertise to construct an anatomical human voxel model with specific properties, the second group contributed their detailed model of an advanced RF coil and the third integrated these parts into one consistent grid model and performed the simulations utilizing their advanced software and hardware resources. Another example of such a 'relay race approach' would be tissue mimicking liquids which were prepared and fully characterized in one laboratory and then shipped to and used by another partner for traceable field measurements in phantoms.

The specific aim of the modelling workpackage was to develop and validate MRI-oriented mathematical models (electromagnetic and thermal fields), to support the assessment and dosimetric evaluation of human exposure to RF fields in an MRI environment, to correlate SAR with temperature elevation and to explore the sensitivity of external field measurements to monitor induced electromagnetic (EM) fields inside the body. This aim, and hence objective 2, was fully achieved.

3.2.1 Development and validation of MRI-oriented mathematical models for EM simulations

Four numerical tools having different characteristics were considered, namely Finite Difference Time Domain (FDTD), Finite Integration Technique (FIT), Boundary Element Method (BEM), and coupled Finite Element – Boundary Element (FEM-BEM) Technique.

For FDTD, a time domain code based on the Yee algorithm, the commercial software SEMCAD-X vs.14.8.5 (SPEAG AG, Zurich) was used. For FIT, based on the integral form of Maxwell's equations, the time domain solver within CST Microwave Studio version 2014 (Computer Simulation Technology, Darmstadt) was used. INRIM developed a first code based on BEM, a technique that solves boundary value problems in their integral form by adopting the Green function as a spatial reconstructor. To overcome the limits of BEM in processing highly inhomogeneous models, an original hybrid FEM-BEM field formulation, working in the frequency domain, was also developed [1-3]. The FEM-BEM code is available for research purposes on the JRP website.

To validate the models, a laboratory setup enabling electromagnetic field measurements to be made in a phantom mimicking the properties of human tissues at MRI radio-frequencies was developed. The phantom consisted of a cylindrical container (diameter 240 mm, height 240 mm) filled with a tissue-simulating liquid (TSL) and was located within a structure which supported the field source and the gantry for positioning the field probes within the liquid (Fig. 3.2-1).

Large metallic bodies can be located within the phantom to simulate the presence of passive implants and to monitor the field distribution distortions around the object. The electrical properties of TSL were measured in the frequency range from 50 MHz to 300 MHz at several temperature values (between 10 °C and 27 °C). Two antennas with different shapes and dimensions similar to a surface MRI RF coil were used to radiate the phantom. A small loop antenna (#1), consisting of a single turn of 6 cm diameter, generated a magnetic field in air of 1 A/m at a distance of 20 mm along the loop axis. A larger (120 $\times$ 105 mm^2) square shape antenna (#2), generated a magnetic field of 2 A/m at a distance of 43 mm along the loop axis.

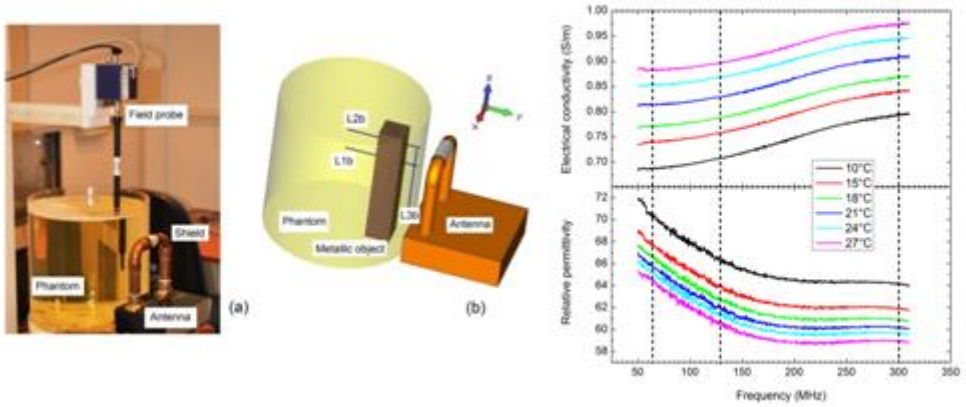

Fig. 3.2-1 *Left: view of the experimental setup with the antenna. Center: scheme of the phantom. Some of the lines of investigation, L1b, L2b and L3b, are indicated. Right: dependence of TSL electrical conductivity and relative permittivity on frequency and temperature.*

E- and *H*-field vectors were measured within the liquid using isotropic probes (H3DV8 *H*-field probe and ER3DV6 *E*-field probe by SPEAG AG, Zurich). A measurement uncertainty budget was estimated, taking into account i) possible temperature oscillations during the measurement stage, ii) possible positioning errors of the field probes and iii) probe inaccuracy. Maximum uncertainties of about 30 % (coverage factor k = 2) were associated with measurements regarding electric and magnetic field amplitudes.

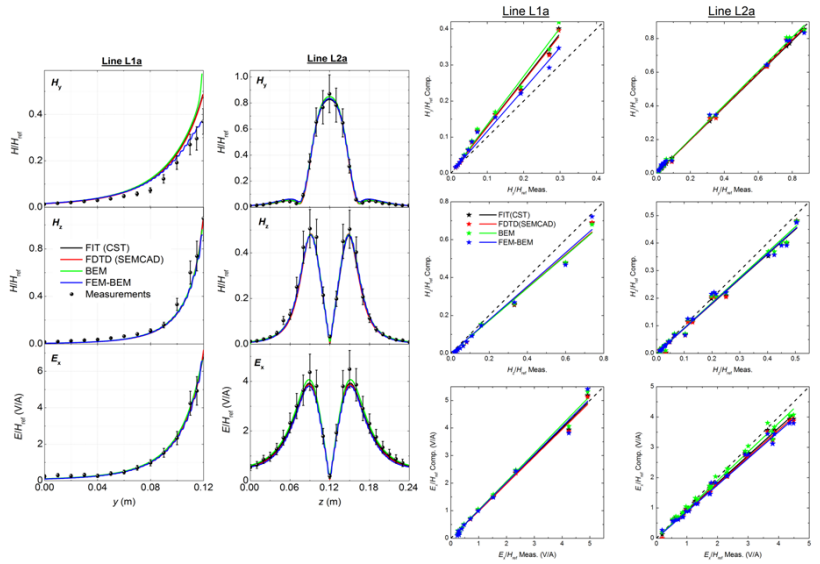

(a) (b)

Fig. 3.2-2 *(a) Comparison among measured and computed normalized fields with the phantom radiated by the antenna #1 at 64 MHz. On the left H_y/H_{ref}, H_z/H_{ref} and E_x/H_{ref} along line L1a, on the right H_y/H_{ref}, H_z/H_{ref} and E_x/H_{ref} along line L2a. A coverage factor k = 2 has been associated to measurement uncertainties. (b) Computational results (C) plotted versus the corresponding measurement points (M) and fitted by linear interpolation (C = a·M), corresponding to data reported in panel (a) (antenna #1 at 64 MHz).*

FDTD, FIT, BEM and FEM-BEM were used to simulate several exposure conditions (antenna #1 and #2, at 64 MHz, 128 MHz and 300 MHz) and configurations (with and without metallic object, relative position between source and phantom, etc.). For each case, magnetic and electric field components were computed and measured along relevant investigation lines. An example of the comparison is

shown in Fig. 3.2-2a, where results are rescaled to the reference value of the magnetic field H_{ref} computed in a selected point close to the source. For each case, computational results (C) have been plotted versus the corresponding measurement points (M) and then fitted by linear interpolation ($C = a \cdot M$), see for example Fig. 3.2-2b, derived from computational and experimental data reported in Fig. 3.2-2a. The parameter of the linear fit, a,, was determined by least-square minimization, and provides a quantitative estimation of the overall quality of the modelling result. A value of $a > 1$ indicates overestimation of computations, while $a < 1$ underestimation. An expanded uncertainty $U(a)$ is associated to this parameter, following the propagation error rules.

Considering the overall values of the parameter a as a statistical datum, the frequency distributions are reported in Fig. 3.2-3. The ratio N_a/N_{tot} is representative of the data frequency; N_a is the number of values found in the corresponding range of parameter a and N_{tot} the total number of results. Results show a satisfactory quantitative agreement between experimental and computational, although the differences increase as the frequency increases. Worst case discrepancies in modelling predictions of 30 % were found for the E- and H-fields, associated with large field gradients obtained in the presence of metallic objects that simulated in a very simple way the presence of an implant. More details and result discussion are reported in Ref. [5].

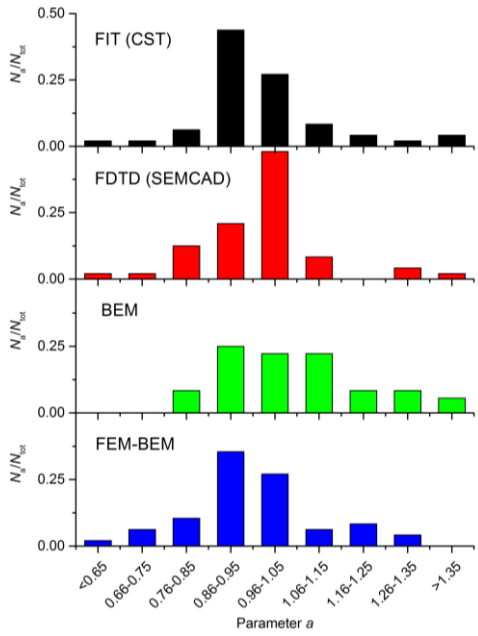

Fig. 3.2-3 *Frequency distribution of parameter a for the considered computational methods. N_a is the number of values found in the corresponding range of parameter a and N_{tot} is the total number of results.*

3.2.2 Correlation between local SAR and temperature elevation

A thermal module, based on the Finite Element technique and Pennes' bioheat equation, was developed and integrated within the FEM/BEM electromagnetic solver. It simulates steady-state temperature elevation in human tissues under continuous exposure conditions and adopts the temperature elevation as unknown, which avoids the need to know the initial temperature distribution and the metabolic rates in tissues.

Preliminary validation of numerical simulations was performed by comparing the results with those obtained by the SEMCAD-X vs.14.8.5 software. A large number of simulations were carried out using the Duke anatomical human model (IT'IS Virtual Family), including bilateral implants, exposed to the RF field at 64 MHz, 128 MHz and 300 MHz.

Correlation between local energy deposition in tissues and related temperature elevation was studied for the case of exposure of the human head to the RF field generated by a generic birdcage coil. To this aim, Duke's model head was considered (voxel resolution of 2 mm). The input RF power was set to generate a B_1^+ field of 1 µT at the isocenter of the unloaded coil. At 64 MHz the magnetic flux density was almost unchanged by the presence of the head and shoulders (Fig. 3.2-4a), but higher perturbations occurred at 128 MHz (maximum B-field up to 1.8 µT). The surface B-field was consequently modified,

as shown in Fig. 3.2-4b, which reports the RMS-value (monitored by a three-axial field probe) and its variation ΔB with respect to the unperturbed case. The maximum variation, at 128 MHz, is found in the neck region, but this is almost independent of the frequency.

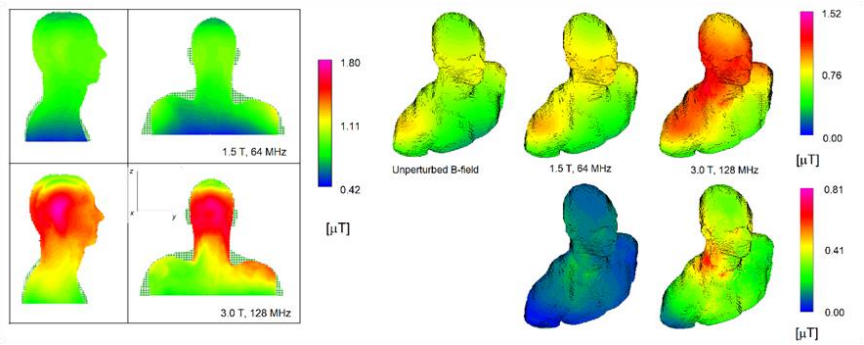

(a) (b)

Fig. 3.2-4 *Head exposure to an MRI RF field: (a) local distribution of B-field at 64 MHz and 128 MHz in the sagittal and coronal sections; (b) B-field over the head surface: from left to right, the unperturbed field and the field at 64 MHz and 128 MHz. In the lower panels, the variation ΔB with respect to the unperturbed case is shown.*

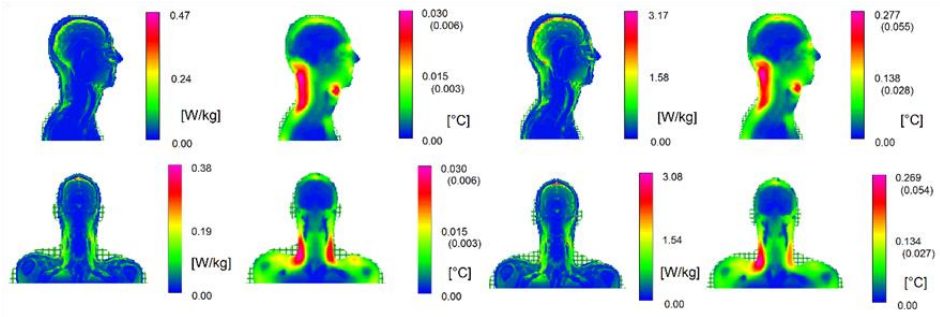

(a) (b)

Fig. 3.2-5 *Simulations at 64 MHz (a) and 128 MHz (b). From left to right, the local SAR and the temperature elevation are shown in the sagittal section (upper) and in a coronal section (lower). Temperature elevations in brackets are rescaled for an RF duty cycle of 20 %.*

Assuming an MRI examination of 30 minutes and a typical tissue time constant of 6-7 minutes, steady state thermal simulations for an RF duty cycle of 20 % were performed. Local SAR and steady-state temperature elevation in sagittal and coronal sections are shown in Figs. 3.2-5. Since the temperature increase θ is strongly affected by the perfusion coefficient (relatively low in the neck region), there is no direct spatial correlation between local SAR values and θ. The maximum temperature increase, for B_1^+ = 1 μT at the isocentre, are 6×10^{-3} °C and 55×10^{-3} °C at 64 MHz and 128 MHz, respectively. Values can be scaled to any B_1^+ according to $\Delta T \propto (B_1^+)^2$.

Table 1.I summarizes the results obtained from the simulations. For each frequency *f*, the average SAR (over the entire head) and the maximum local SAR, computed using the 99th percentile (SAR^{99th}), are reported. The corresponding maximum variation of the *B*-field amplitude over the head surface ($\max \Delta B_S$) is recorded. The average SAR is strongly correlated with $\max \Delta B$, if rescaling with frequency is considered. Indeed, the parameter $SAR^{avg}/(\max \Delta B_S \cdot f)$ is almost constant, with variations of ~10 %. Some correlation is also found with respect to the local SAR; variations of parameter $SAR^{99th}/(\max \Delta B_S \cdot f)$ are found within 20 %.

Table 1.I. *Summary of results. See text for definition of quantities*

f (MHz)	SAR^{avg} (W kg^{-1})	SAR^{99th} (W kg^{-1})	$\max \Delta B_S$ (μT)	$\max \Delta B_S$ @ 3.2 W/kg (μT)	$\frac{SAR^{avg}}{\max \Delta B_S \cdot f}$ (W kg^{-1} T^{-1} Hz^{-1})	$\frac{SAR^{99th}}{\max \Delta B_S \cdot f}$ (W kg^{-1} T^{-1} Hz^{-1})
64	0.74	3.87	1.75	3.64	0.007	0.035
128	6.4	32.1	6.37	4.50	0.008	0.039
300	49	255	17.5	4.47	0.009	0.049

3.2.3 Summary RF electromagnetic field calculations

- An assessment and comparison of different numerical techniques for RF simulations was made using new concepts, developed within the project, as well as commercially available software. Depending on details of the problem, each technique can over or under-estimate the real (measured) field values. Nevertheless it was possible to draw some general conclusions about the suitability of a given method or software package for certain classes of problems.
- To assess the validity of the numerical results, comparisons of computations and measurements were performed under controlled laboratory conditions. Generally, they show good qualitative and satisfactory quantitative agreement. Worst case discrepancies of up to 30 % were found for the RF electromagnetic fields near metallic implants. Within the scope of the present project this is sufficient but ultimately an agreement within 10 % is desirable for all cases.
- When studying thermal effects in tissue only a weak spatial correlation was found between local RF power deposition (the so-called specific absorption rate, SAR) and resulting temperature increase. This finding is practically highly relevant, since most existing safety standards limit SAR, the heating term, while they want to limit temperature. The difference is explained by tissue perfusion which provides an effective internal cooling mechanism that is not spatially correlated to the SAR distribution.

References 3.2

[1] O. Bottauscio, M. Chiampi, L. Zilberti, IEEE Trans. Magn., Vol.50, No.2, 2014, 7025504.
[2] O. Bottauscio, M. Chiampi, L. Zilberti, Engineering Analysis with Boundary Elements, Vol. 49, 2014, pp. 15-21.
[3] O. Bottauscio, M. Chiampi, J. Hand, L. Zilberti, IEEE Trans. Magn., Vol. 51, No. 3, 2015, 5100904.
[4] D. Giordano, L. Zilberti, M. Borsero, M. Chiampi, O. Bottauscio, IEEE Trans. Magn., Vol. 50, No. 11, 2014, 5101504.
[5] O Bottauscio, A M Cassarà, J W Hand, D Giordano, L Zilberti, M Borsero, M Chiampi, G Weidemann, Phys. Med. Biol. 60 (2015), 5655-5680.
[6] L. Zilberti, O. Bottauscio, M. Chiampi, J. Hand, H. Sanchez Lopez, R. Brühl, and S. Crozier. Magn Reson Med 2015. doi: 10.1002/mrm.25687.

3.3 Motion induced low-frequency fields and currents

The work on objective 3 was partly built on results described in the previous subsection. It was mostly done by the Turin group (INRIM) with some input data, in particular field maps, provided from Berlin (PTB). All aspects of objective 3 were achieved within the lifetime of the MRI Safety project.

3.3.1 Development of a mathematical and numerical framework

Activities started about 6 months into the project and were initially based on a computational tool [1] previously developed by INRIM in collaboration with Politecnico di Torino. The tool, written in terms of field quantities, is a particular application of the vector analogue of Green's theorem in time-domain. It

was simplified for more general use (for more details see the explanation given in [2]) with reference to the specific features of the problem, namely the hypotheses of:

- absence of ferromagnetic and highly conductive objects in the computational domain;
- magnetic field impressed by the sources (i.e. not perturbed by the currents induced in the body);
- negligible dielectric effects.

The formulation for the tool has been written in the co-moving reference frame of the body, it exploits the time derivative of the magnetic flux density as a driving term and is solved numerically through the Boundary Element Method (BEM). The quasi-stationary operating conditions and the restriction to rigid motions led to a real BEM matrix, which is invariant with respect to the considered time-step. The results can be scaled linearly with both the flux density level and the instantaneous value of the speed. The computational scheme inherently avoids questionable approximations made in other approaches (see for example the analysis developed in [3]); moreover, some critical comments raised in [4] could be convincingly disproved [2]. After the discussions contained in [2-4], a group from the University of Queensland (UQ, Australia) expressed its interest to cooperate with the consortium in the area of motion-induced fields. The expertise gained allowed the consortium to solve the problem contained in the formulation developed at UQ (based on a Finite Difference Time Domain scheme and criticized in [3]) and led to a joint paper [5], as well as a presentation at the ISMRM 2014 conference [6].

The BEM code was implemented into a Fortran90 Visual Studio Environment and operated on a classical CPU hardware platform. This computational tool was then used in [7] to study the exposure of a simplified and homogeneous human model (a 3-dimensional axial symmetric version of the “reference man” described in Standard EN 62226-3-1, see Fig. 3.3-1), moving through the stray field produced by realistic MRI scanner geometries (tubular, open ironless with vertical axis and open ironless with horizontal axis). Such field distributions were obtained through computation starting from verisimilar coil designs. Their suitability to describe real exposure scenarios was checked against experimental values obtained by PTB under a non-disclosure agreement allowed by a manufacturer.

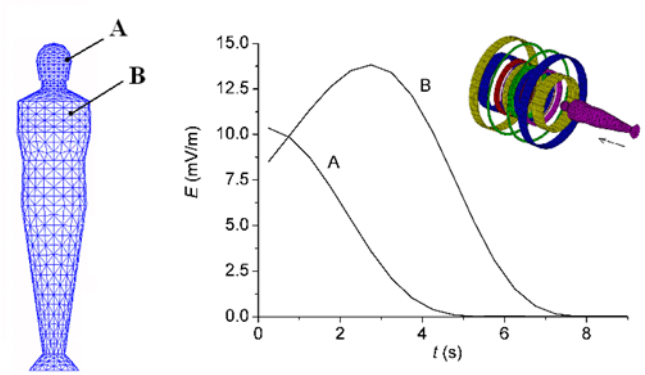

(a) (b)

Fig. 3.3-1 *Simplified human model (a) and example of computed motion-induced electric field when the body enters a 1.5 T scanner with a uniform speed equal to 0.1 m/s (b).*

Realistic trajectories and some complex motions (e.g. bowing) were considered and the approximation introduced by a body truncation (useful to reduce the computational burden) was analyzed. At this level, when no specific exposure guidelines were available, the results were presented in terms of peak and average values of the time-dependent induced electric field, but the whole signal was also studied in order to identify the harmonic content. Apart from the quantification of the induced field in itself, the main results coming from this first survey can be summarized as follows:

- In general, motion-induced fields are higher for abrupt rotations compared to translational movements.
- Due to their strong field gradient, open scanners can have induction effects as high as the ones obtained for tubular scanners, despite their lower nominal flux density.

- In order to get reliable results in the head, the simulation of the head alone is not enough, but a larger portion of the body (e.g. the upper part, starting from the waist) must be considered.

The main drawback of this first approach is due to the numerical method. Indeed, BEM is not best suited to handle high-resolution anatomical models, because the latter are strongly heterogeneous and would require the use of a large number of boundary surfaces, reducing both the computational efficiency and the numerical accuracy. For this reason, a change in the modelling strategy was introduced and a new formulation, more suitable to handle voxel-based human models, was developed and implemented. The new formulation is written again in the co-moving reference frame, but using an induced electric scalar potential as an unknown and the time derivatives of a magnetic vector potential (directly computed starting from the features of the sources) as a driving term. Its numerical solution is set following the Finite Element Method (FEM), directly using the hexahedral voxels of the anatomical model as elementary cells. The implementation has been carried out according to a parallelized scheme, which allows the code to run on GPU architectures. Most of the working hypotheses remain the same as for the previous BEM formulation (rigid motion, unperturbed magnetic field), but the dielectric component of the induced current is no longer neglected, obtaining a more general description of the problem. This feature makes the scalar potential a state variable, requiring a time-stepping scheme (e.g. Crank-Nicolson algorithm) to update its value at each computational step. In addition, the new term introduces, within the computation of the induced field, a contribution with a direct dependence upon acceleration. Thanks to such facility, never before implemented in computational tools for motion-induced fields, it has been possible to analyze the effects associated to the dielectric currents, the dispersion of tissue parameters (both conductivity and permittivity) and, most importantly, accelerated/decelerated motion phases on the induced electric field. All these analyses are collected in [8], where the computations were performed for the “Duke” anatomical model (i.e. a voxel-based dataset representing an adult male composed of 77 different tissues). The dielectric properties of the tissues have been extrapolated from the IT'IS database (http://www.itis.ethz.ch/virtual-population/tissue-properties/overview/), by applying a 4th-order Cole-Cole dispersion model, which provides extremely high values of relative permittivity (e.g. 50×10^6) for some materials in the frequency band of interest (i.e. around 1 Hz). Note that such values are controversial and affected by very high uncertainty levels, but, at the current state of the art, they are the only available in literature and this justifies the attention towards their effect on motion-induced fields. The analysis has made the following findings:

- On the whole, an almost direct correlation between the magnitude of the motion-induced fields and the instantaneous speed value exists (see Fig. 3.3-2); this requires the use of realistic trajectories (including acceleration and deceleration phases) to correctly quantify the phenomenon.
- Despite the extremely high permittivity, the effect of dielectric currents is negligible if the induced electric field is used as a metric to quantify the exposure (the effect would be stronger on the total current density). At the same time, the effect of the dispersion in frequency is also found to be negligible (over a reasonable band of interest) when considering the electric field. These findings partially remove the need for an accurate knowledge of the parameters.
- As for the cases previously obtained through the BEM approach, the use of a truncated human model is allowed only if the model includes not only the head but the complete upper torso. However, in the case of this more realistic heterogeneous model, the stability of the results is reached more easily (e.g. by truncating the body just below the shoulders), because the induced currents tend to circulate more locally.

3.3.2 Adapting the project to external developments: the new ICNIRP guidelines

During the lifetime of the project, March 2014, the International Commission on Non-Ionizing Radiation Protection (ICNIRP) published the document "*Guidelines for limiting exposure to electric fields induced by movement of the human body in a static magnetic field and by time-varying magnetic fields below 1 Hz*" (available at http://www.icnirp.org/en/publications/index.html). In response to this highly relevant external development, one of the scheduled activities (i.e. identification of the relevant dosimetric parameters) was adapted. The new focus was on the protection strategy given by ICNIRP, which is based on two basic restrictions:

- The maximum change of magnetic flux density experienced during any 3 s time interval (to prevent vertigo and nausea).

- The peak of the motion-induced electric field (to avoid nerve stimulation and magnetophosphenes). Since the waveform of motion-induced fields is typically non-sinusoidal, the whole frequency spectrum of the motion induced electromagnetic fields has to be taken into account. This is applied according to the “weighted peak approach”, defined in previous Guidelines.

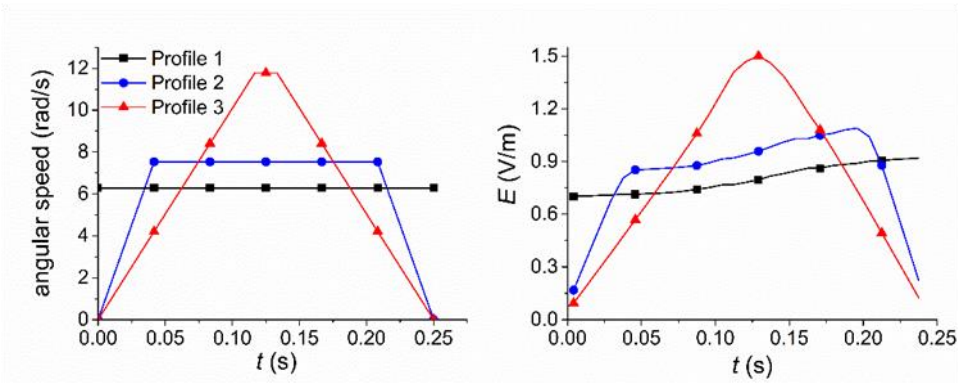

(a) (b)

Fig. 3.3-2 *Abrupt rotation of a human head around its vertical axis (90° in 0.25 s), through a uniform and unitary flux density parallel to ground: considered angular speed profiles (a) and corresponding 99th percentile of the motion-induced electric field in brain (b).*

In order to carry out the final exposure assessment according to these limits, the FEM code has been enriched with post-processing facilities able to provide the exposure indices as required by ICNIRP. In particular, different possibilities of computing the *E*-field exposure index (i.e. implementing the weighted-peak approach via a Discrete Fourier Transform or based on signal processing realized by a filter) were explored. It could be shown that these two techniques do not always give compatible results, even though both of them conform to the guidelines. This outcome, together with other critical aspects of the new guidelines which were discovered during the analysis, calls for further specifications from the standardization bodies.

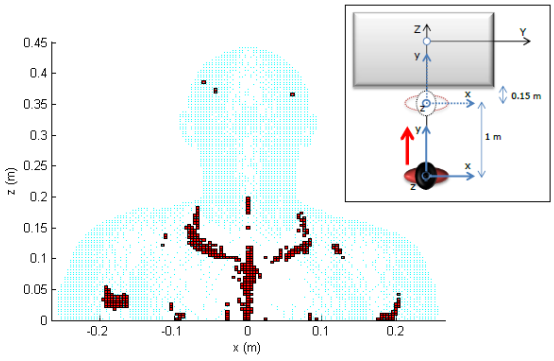

Fig. 3.3-3 *Voxels where the exposure index for the induced electric field exceeds the ICNIRP limits in case of a longitudinal translation towards the bore of a 3 T scanner (1 m in 1 s, with non-uniform speed). The non-zero number of such voxels means that the depicted trajectory violates the ICNIRP guidelines.*

After the above-mentioned preliminary analysis, a wide exposure assessment to motion-induced fields was carried out, focusing attention on the effects induced inside the head (see for example Fig. 3.3-3). Two exposure scenarios, involving a traditional tubular 3 T scanner and a 1 T open ironless scanner with vertical axis, were selected. Realistic movements near the bore of these MRI platforms have been considered (both translations and rotations, including some motions useful to simulate MRI-guided surgery), and three different statures of the human model have been adopted, for a total of 42 simulated cases. The results indicate that a violation of the ICNIRP limits for the maximum variation of the flux

density vector is unlikely for common movements performed during clinical practice (only movements which put the head of the operator close to the coils should be able to exceed the limits). The possibility of exceeding the limit for the induced electric field is higher, but violations of the basic restriction should only occur when a human body (in particular of low stature) moves in very close proximity to the magnet. In this case, abrupt head rotations appear to be the most “critical” situations. Whenever proximity to the bore is necessary, the only safety rule to reduce the onset of biological effects seems to be the reduction of the speed of motion. On the contrary, an increase in the speed of motion can raise the probability of biological effects more than linearly, because typically it extends the harmonic spectrum of the induced signal towards higher frequencies (associated to lower exposure limits). A summary of this final exposure assessment, the first performed according to the new ICNIRP Guidelines, will be presented at the COMPUMAG 2015 conference (Montreal, June 2015) and also be made available through an extended paper currently under preparation.

3.3.3 Summary Motion induced low-frequency fields and currents

- Advanced computational tools were developed to determine motion induced low frequency fields and currents in anatomical body models by numerical simulations.
- The 2014 International Commission of Non-Ionising Radiation Protection (ICNIRP) guidelines request an ‘exposure index’ estimation for motion induced fields by applying a suitable weighting approach. These guidelines are highly relevant as ICNIRP is the preferred source of reference for EU legislators. The project demonstrated that different weighting approaches, even though all guideline conforming, can give different results. This highlights the need for an amendment of the guidelines in this respect.
- The previously developed computational tools were applied in a broad investigation considering a variety of MRI magnets and realistic motion trajectories. The results showed: (i) no violation of the ICNIRP limits when the subject is performing common movements during clinical practice, (ii) a violation of the ICNIRP limits, in contrast, is possible when the subject moves abruptly in close proximity to the magnet.

References 3.3

[1] Chiampi M., Zilberti L., IEEE Trans Biomed Eng, 58, 2787-2793 (2011).
[2] Chiampi M., Zilberti L., IEEE Trans Biomed Eng, 60, 882-883 (2013).
[3] Cobos Sanchez C., Glover P., Power H., Bowtell R., Phys Med Biol 57, pp. 4739–4753 (2012).
[4] Cobos Sanchez C., IEEE Trans Biomed Eng 60, 880-881 (2013).
[5] Trakic A., Liu L., Sanchez Lopez H., Zilberti L., Liu F., Crozier S., IEEE Trans Biomed Eng 61, 784-793 (2014).
[6] Trakic A., Liu L., Sanchez Lopez H., Zilberti L., Liu F., Weber E., Crozier S., Proc. ISMRM 22, 4428 (2014).
[7] Zilberti L., Chiampi M., Health Phys 105, 498-511 (2013).
[8] Zilberti L., Bottauscio O., Chiampi M., IEEE Magn Lett, 6, 1500104, (2015).

3.4 Emerging technologies: parallel transmission (pTx) and ultrahigh fields

This subsection summarizes the results obtained in pursuit of objective 4. The objective was fully achieved mainly due to the combined work of the Berlin (PTB) and London (KCL) group. The research on pTx and ultrahigh fields represents a more application oriented objective and extensively utilized results obtained under the more fundamental objectives 1 "RF measurements" and 2 "RF simulations", as described in subsections 3.1 and 3.2, respectively. Substantial indirect contribution from Turin (INRIM) must also be acknowledged for the present context, therefore.

3.4.1 Procedures and tools for comprehensive RF safety calculations in pTx MR systems

The development of a simulation infrastructure which allows comprehensive RF safety calculations for multichannel transmit MR systems (pTx) represents another key result from this project. To achieve this goal PTB developed a number of procedures and tools to account for the specific RF related hazards associated with pTx MRI systems in particular when using ultrahigh fields. The considered procedures and tools utilize datasets generated by commercial FDTD solvers but are completely written in house.

In addition to the planned activities a GPU accelerated code for the Pennes' Bioheat Equation was written by PTB to correlate peak spatial SAR with local tissue temperature.

First of all a tailored FDTD mesh generation tool was implemented using voxel models and tissue properties from the common available IT'IS database. The tool generates FDTD meshes for both EMF and thermal simulations. The mesh generation assigns tissue types with higher conductivity a higher priority avoiding discretization artefacts due to disruption of internally connected tissue structures.

Furthermore, a procedure for the proper design of pTx coil models was established. Since tuning, matching and decoupling networks are incorporated later by co-simulation [1], the coil model includes additional ports for decoupling of coil elements. Thus, the total number of ports in the model of a typical eight channel pTx coil is 24 (8 feeding ports, 16 decoupling ports). For each port a separate FDTD run is necessary resulting in typically 0.5 GB to 1 GB of 3D steady state field data per port. From steady state port voltages and port currents the impedance matrix and S-parameter matrix are calculated and used as input for the subsequent co-simulation.

PTB developed a co-simulation framework for the tuning/matching/decoupling of pTx coils including intrinsic coil losses. As a result the complete power balance and 3D field superposition can be calculated not only for arbitrary driving voltage vectors but also for different tuning/matching/decoupling parameters. From 3D field superpositions, distributions of all relevant field quantities can be deduced, e.g. B_1^+, B_1^-, E_1, local SAR and local SAR averaged over 10g.

For RF safety considerations the peak spatial value of the 10g averaged SAR ($psSAR_{10g}$) is the most relevant parameter as documented exposure limit values for this quantity must not be exceeded [2]. To simplify access to $psSAR_{10g}$ the 3D power correlation matrix ("Q-matrix") [3] is calculated using all previous data. Once this matrix is known, the SAR values for any driving condition of the pTx system can easily be obtained from the bilinear form uQu, where u is the vector containing the complex driving voltages for each channel.

In principle, the Q-matrices must be computed for each spatial coordinate of the 3D volume under consideration. This represents very large data sets and thus makes the application of data compression schemes like the method of 'Virtual Observation Points' (VOPs) [4] highly desirable. The Berlin group developed and implemented an algorithm to calculate VOPs with known overestimation errors [5]. An important finding was that the eigenvectors of VOPs represent the most critical voltage driving vectors for the pTx system in terms of local SAR. This includes the 'worst case' scenario, of course, i.e. the one single driving condition producing the highest possible $psSAR_{10g}$ value. Thus, VOPs can be used as versatile test-bed for safety assessments of pTx MR systems.

Table 3.4-I *Simulation results for an 8-channel pTx coil array at 7 T: Compliance with the 20 W/kg local SAR limit of IEC 60601-2-33 Ed.3 can be achieved by limiting the forward power for each channel to 1.5 W. Also the volume SAR limit for the head, calculated from the largest eigenvalue of the volume averaged Q-matrix, never exceeds 60 % of the limit value of 3.2 W/kg in this scenario. Limiting the* overall *forward power, instead, to the same value of 8 × 1.5 W = 12 W but now without any per-channel constraints SAR values of up to 35.5 W/kg $psSAR_{10g}$ are obtained, i.e. almost 1.8 times the limit value.*

	'Duke'	'Ella'	phantom
upper limit of total absorbed power vs. total forward power	0.881	0.823	0.863
upper limit of 'head' SAR @1.5W per channel	1.89 W/kg	1.89 W/kg	1.49 W/kg
'worst case' SAR_{10g} for a total forward power of 8 x 1.5W = 12W	35.5 W/kg	30.2 W/kg	26.8 W/kg
upper limit of SAR_{10g} @1.5W per channel	19.7 W/kg	18.7 W/kg	15.3 W/kg

A key result of this approach was the finding that the determination of $psSAR_{10g}$ at 7T is unfavourably sensitive to model details when relying on measured multi-channel driving voltages. Hence, PTB developed a procedure for the calculation of an upper limit of $psSAR_{10g}$ for a fixed individual channel forward power [6]. This approach is slightly over-conservative, i.e. sacrifices some performance, but it was shown that demonstrating compliance with IEC 60601-2-33 is much simpler and more robust following this approach.

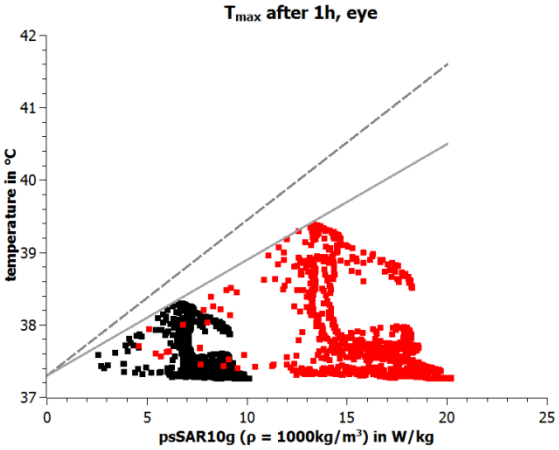

Fig. 3.4-1 *Peak steady state temperatures vs. $psSAR_{10g}$ for eye tissue: 2 × 873 different voltage vectors were used, total forward power was 8 W (red squares) or 4 W (black squares). The solid line indicates an upper limit extrapolation, the dashed line is the extrapolating line for the temperature-wise most sensitive tissue type, a (virtual) combination of muscle, skin and fat. From [7].*

PTB's aforementioned GPU accelerated code to solve Pennes' Bioheat Equation is based on the OpenACC framework of the PGI Accelerator compiler suite (The Portland Group, Beaverton, OR). To avoid any discretization artefacts the identical FDTD mesh is used for thermal as well as for EMF calculations. This ensures that the heat generation terms match exactly with the right tissue type. This fast implementation of Pennes' Bioheat Equation allows to perform >1000 simulations in a reasonable time. Maximum steady state temperatures were determined for different groups of tissue types with different susceptibility to temperature rise [7]. This is important when accessing the risk of tissue damage for a large set of local SAR scenarios as given by the eigenvectors of the VOPs.

3.4.2 Characterization of 3T and 7T pTx coils

Using the versatile measurement infrastructure developed within the project (see Sec. 3.1.1) PTB characterized one 3T and two 7T 8-channel pTx head coil arrays. A key result is the determination of the power balance of a commercial 7T 8-channel pTx head coil with internal shielding, including the power radiated into the far field. The maximum radiated power for this particular coil was determined as 1 % of the overall forward power. The maximum occurs when driving the elements with a phase increment of 45 degrees, i.e. in a circularly polarized (CP) mode. This experimental finding is consistent with recent simulation data [8]. The low portion of radiated power is due to the shielding of the individual elements. This somewhat atypical design feature simplifies the RF safety assessment of this particular coil.

3.4.3 pTx for SAR managing in the presence of metallic implants

PTB developed a new method to control implant heating by transmit array coils [9]. Utilizing the additional degrees of freedom of pTx coil arrays the hazard of excessive local tissue heating due to metallic implants can be mitigated. In this Q-matrix approach the single Q matrix associated with the proximate tissue volume of a metallic implant can be used to determine the 'worst case' steering conditions for implant heating. A projection technique was applied to calculate new steering conditions which resulted in much lower implant heating. The efficacy of this method was demonstrated by EMF and thermal simulations using a 7T 8-channel head coil model.

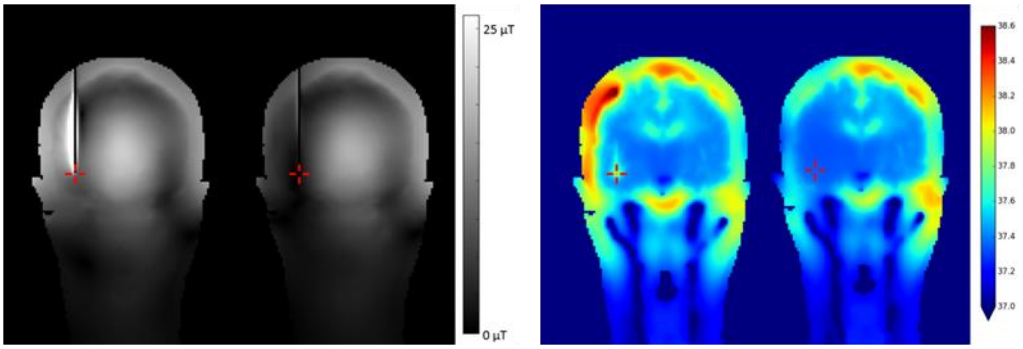

Fig. 3.4-2 *Left: Coronal maps of $|B_1^+|$ for CP-mode excitation (left) and using the projection method (right) at 1 kW of total forward power. $|B_1^+|$ artefacts near the implant are due to induced RF currents. For the projection method these artefacts are effectively suppressed. The red cross indicates the position of the wire's tip. Right: Coronal maps of steady state temperature for CP-mode excitation (left) and using the projection method (right) at 20 W of total forward power. No significant implant heating occurs when using the projection method. From [9].*

PTB performed additional measurements of RF currents in a conductive wire as metallic implant using a 3T 8-channel pTx head coil and the body phantom developed in the JRP. With this experimental setup the newly developed method to control implant heating by transmit array coils was verified.

3.4.4 Summary: Emerging technologies - parallel transmission (pTx) and ultrahigh fields

- The advanced simulation infrastructure for RF safety calculations (see above) was applied to the case of ultrahigh fields (e.g. 7 T) where the field distributions become inhomogeneous and conventional safety measures fail. The measurement method based on calibrated RF field probes was utilized to validate the simulation results in this case, too.
- Radiation into the far-field is an additional possible dissipation path for RF power which must be correctly predicted by a numerical simulation. This mechanism is negligible at conventional field strengths but has to be accounted for at ultrahigh field strengths, i.e. 7 T or above. A method for the measurement of the radiated RF power at 7 T was devised and successfully tested. This way, the last missing quantity in the power balance equation became accessible and the metrological concept to provide traceable measurements of the RF electromagnetic fields associated with an MRI exam was completed.
- An additional challenge particular to pTx systems is the virtually unlimited number of possible set-points to be considered in a safety assessment. To reduce this complexity to a treatable level a strategy was improved and implemented, allowing to identify a small subset of the most critical pTx parameter settings. Any safety limits sufficient for these critical cases will automatically suffice for all other conditions possible. With this extra step it is now possible to apply the aforementioned safety concept based on validated numerical simulation to the pTx case, as well.
- The concept described above is generally applicable and valid. Its practical supervision requires some extra hard- and software, however, to analyse the state of the pTx system in real time and to perform on-the-fly comparisons with pre-set safety limits. An additional, simplified version of that pTx safety strategy was therefore developed. It is slightly over-conservative, i.e. deliberately sacrifices some performance, but can be implemented without the need for real-time measurements or simulations, making it robust, reliable, and compatible with existing and certified RF supervision hardware. With this approach it is much easier to demonstrate compliance with the relevant standards on MRI safety.
- It was stated before that potentially hazardous heating of tissue is the real concern about MRI related RF electromagnetic fields and this is unchanged when pTx considered. Soft- and hardware for very fast thermal simulations were thus implemented, allowing to assess the associated temperature rise for the large number of different pTx parameter settings. This gives much deeper insight into patient safety compared to electromagnetic simulations alone.

References 3.4

[1] Kozlov M, Turner R. J Magn Reson 200, 147–152 (2009).

[2] IEC 60601-2-33, ed. 3 (2010).
[3] Zhu Y. Magn Reson Med 51, 775–784 (2004).
[4] Eichfelder G, Gebhardt M. Magn Reson Med 66, 1468–1476 (2011).
[5] Seifert, F.; Ittermann, B.; Proc. ISMRM 21, 2827 (2013)
[6] Seifert, F.; Cassara, A.; Weidemann, G.; Ittermann, B.; Proc. ISMRM 22, 4891 (2014)
[7] Seifert, F., Weidemann, G., Ittermann, B.; Proc. ISMRM 23, 380 (2015).
[8] Kuehne, A.; Goluch, S.; Waxmann, P.; Seifert, F.; Ittermann, B.; Moser, E.; Laistler, E.; Magn Reson Med (2014), dx.doi.org/10.1002/mrm.25493
[9] Seifert, F., Weidemann, G., Ittermann, B.; Proc. ISMRM 23, 3212 (2015).

3.5 Emerging technologies: MRI-accelerator combination

The establishment of methods for dosimetric traceability for the MRI accelerator and assessing its effect on relative biological effectiveness, objective 5, was a joint endeavour of the groups from Delft (VSL) and Braunschweig (PTB). The main contribution from VSL was the development and characterization of an MRI compatible water calorimeter while PTB was mostly concerned with the basic processes of radiation damage to biological tissue in the presence of a strong magnetic field. The joint work made it possible, however, to completely achieve this objective. The commissioning of the newly built calorimeter in the MRI-accelerator at UMC Utrecht was not possible within the lifetime of the MRI Safety project. This was beyond the control of the consortium as it was caused by delays with the first clinical prototype of the MRI-accelerator. As a result the calibration of the detectors was not possible.

With respect to the relative biological effectiveness (RBE) the mean values of the triple differential cross sections (TDCS) were computed for electron scattering with and without magnetic field and found to have no significant difference. The implementation of the magnetic field effects in a track structure code PTra for simulating the footprints of ionizing radiation at the nanometric scale, on the other hand, showed that the orientation of the water molecules affects the energy and direction of the emitted electron. These results were used to generate cumulative probability distributions necessary for the random sampling of the new kinematic parameters of the electron after interaction with the oriented water molecule. The investigation of the potential influence of strong external *B*-fields on the track structure and hence on the RBE of secondary electrons produced by therapy radiation beams in a water phantom was done with respect to the formation of double strand breaks (DSBs). The changes were found to be well within the statistical uncertainties of the track structure simulations. Hence, using a RBE equal to unity with respect to DSB formation is reasonable for all investigated radiation qualities.

3.5.1 The new magnetic field compatible water calorimeter

VSL developed a new transportable water calorimeter as an absorbed dose standard applicable in MRI incorporated treatment machines, illustrated in Fig. 3.5-1. It is replacing the current calorimeters for application in photon beams with energies between 100 kV and 25 MV. In 2012 the calorimeter specifications and conceptual design were made. In 2013 the calorimeter was designed in detail and constructed. Key-features of the new calorimeter are;

- its compact design (based on heat transport simulations) without compromising the thermal characteristics
- its compact measurement equipment,
- fast and efficient on-site operation and
- its ability to measure in horizontal and vertical beams and treatment machines with patient bore sizes larger than 70 cm.

Waterproof dosimeters can be calibrated and characterized directly inside the calorimeter phantom. Non-ferromagnetic metals were used to operate the calorimeter in the magnetic field of an MRI incorporated treatment machine.

For operation in strong *B*-fields, two calorimeter thermistor probes were characterized in the presence of a 1.5 T field of the VSL electromagnet (Fig. 3.5-2). A change in thermistor resistance, R_B, was observed due to the so called magneto-resistance effect, δ_{MR}, with $R_B = R\ (1 + \delta_{MR})$. This results in a correction to the thermistor radiation induced temperature change ΔT of:

$$k_B = = 1 + \frac{1}{(1+\delta_{MR})}\frac{1}{\alpha}\frac{d\delta_{MR}}{dT}$$

With values for δ_{MR} = -4·10^{-5}, thermistor coefficient α = -0.043 K^{-1} and d(δ_{MR})/dT = 8·10^{-7} K^{-1}, this results in a correction of k_B = 1.00002, considered negligible with respect to the target overall D_w uncertainty.

The *Penelope* Monte Carlo (MC) code [1] was used to calculate 3D dose distributions in an MRI-accelerator beam with a 1.5 T *B*-field. MC phase space files were kindly provided by accelerator manufacturer Elekta. These calculations resulted in absorbed dose ratios between glass vessel and water, D_g/D_w of 0.876(3) without *B*-field and between 0.846(3) and 0.878(3) with 1.5 T field depending on its orientation in the beam. It was concluded that the difference in D_g/D_w for the last orientation is negligible.

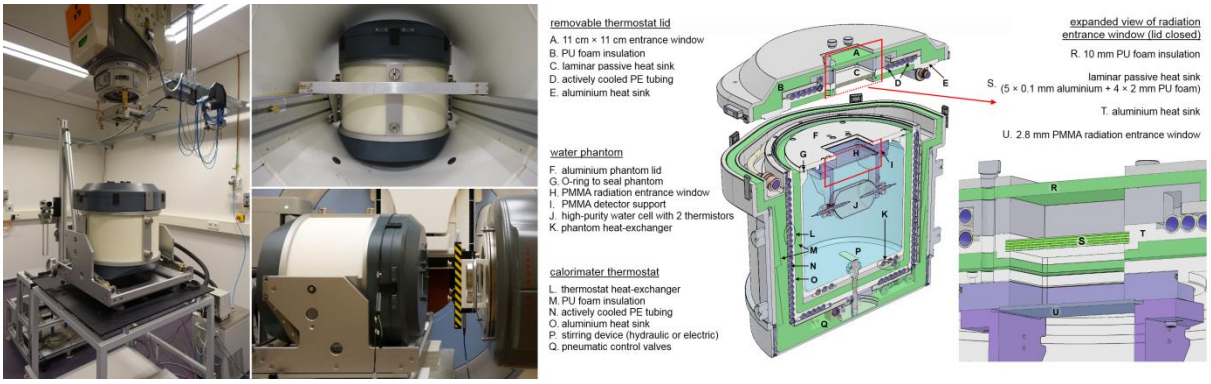

Fig. 3.5-1 *The new calorimeter in the vertical VSL ^{60}Co beam (photo: left), inside the bore of a Elekta Atlantic MRI/linac combination at UMC Utrecht, The Netherlands (photo: top right) and a horizontal beam orientation in front of an Elekta Versa HD accelerator at the Netherlands Cancer Institute in Amsterdam, The Netherlands (photo: bottom right). A schematic cross-section of the calorimeter (illustration: right).*

A calorimeter heat transport model was created in Comsol Multiphysics in order to calculate the heat transport correction due to undesired (excess) temperature effects. Results from the aforementioned 3D dose distribution calculations were used as input to the calculations. The corresponding excess temperature correction was determined as k_{xs} = 0.9954(15).

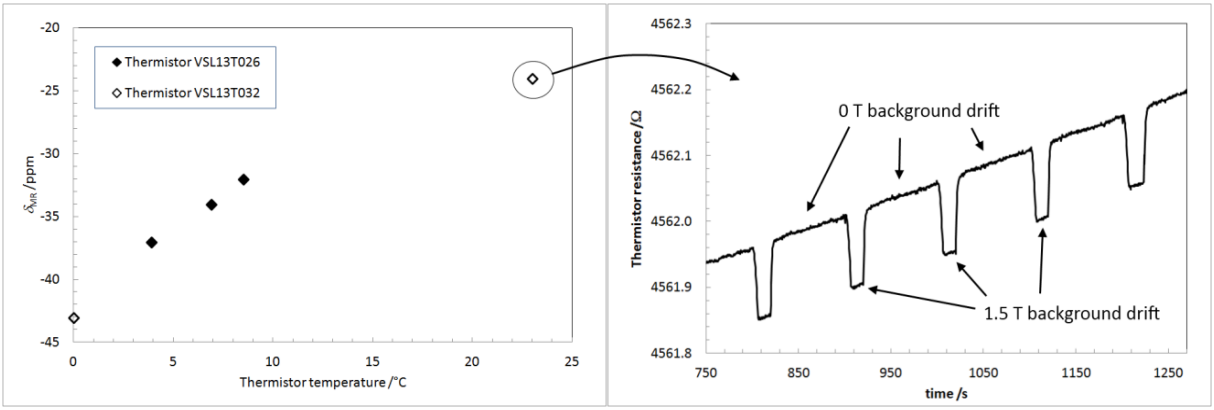

Fig. 3.5-2 *The measured magneto-resistance effect of two thermistors, expressed as δ_{MR} in ppm at temperatures between 0 and 23 °C (right). Illustration of the measurements at room temperature (right).*

The calorimeter has been successfully commissioned in photon beams of ^{60}Co, 6 MV and 10 MV (flattening filter and non-flattening filter) at Netherlands Cancer Institute (Amsterdam, The Netherlands) [2]. Additionally it was used in a BIPM.RI(I)-K6 key-comparison at the National Physical Laboratory (Teddington, United Kingdom) in photon beams of 6, 10 and 25 MV and will be fully commissioned as a

primary standard for MV-photon beams after the results have been released [3]. In November 2014, the water calorimeter was mechanically fitted inside the bore of the prototype MRI linac at UMC Utrecht with the magnetic field ramped down (i.e. 0 T) as shown on the bottom-right photo in Fig. 3.5-1. The new water calorimeter will become an internationally accepted primary standard that is also capable of establishing the absorbed dose to water in the presence of a strong magnetic field. These were essential steps in order to achieve the project objectives and to establish traceability for dose-to-water determination in MRI incorporated treatment machines.

A number of eight ionization chambers (3 × NE2571, 3 × NE2611A, 2 × PTW30013) were calibrated in ^{60}Co as a starting point for the determination of the chamber specific correction factor k_Q in MV photon beams such as the Elekta MRI-accelerator. Unfortunately, due to the aforementioned delays in the realization of the UMC Utrecht MRI-accelerator, the determination of *B*-field corrections was not possible. This would have been the next important step towards bringing traceability to the radiotherapy clinic. A benchmarking method for dose simulations in MC codes in the presence of a *B*-field was developed and submitted for publication [4]. This is of key value to the modelling and application of detectors in MRI-accelerators.

3.5.2 Transport and biological effectiveness of radiation in a strong magnetic field

The mean values of the triple differential cross sections (TDCS) were computed for electron scattering with and without magnetic field and compared in order to evaluate whether the interaction cross sections used in Monte Carlo (MC) codes for the simulation of low energy secondary electron transport need to be modified. Conventionally, the asymmetry of the water molecule is not accounted for in MC codes. Instead, the value of the TDCS obtained by averaging the values of the differential cross sections over the molecular orientation is used. The consortium computed the TDCS in the presence of a *B*-field, based on the assumption that the water molecules are diamagnetic. Thus the overall energy of a water molecule depends on the relative orientation with respect to the *B*-field. For liquid water in equilibrium conditions, neglecting the hydrogen bonds and the free rotation of the molecules, the energy of the water molecules is distributed according to the Boltzmann function. The Boltzmann distribution function depends on the energy of the molecules and hence a partial orientation in the presence of the *B*-field is expected. This Boltzmann distribution as well as a set of differential cross sections (DCS) values were computed for electron elastic scattering and ionization on water for various molecular orientations and used to calculate the TDCS in the presence of a *B*-field. The comparison of the TDCS with and without magnetic field showed no significant difference, however, for magnetic field strengths of 1.5 T and 3 T.

PTB has modified the existing Penelope MC code by implementing the Lorentz force acting on the trajectories of the secondary electrons [1] to predict the 3D macroscopic dose distribution of an MRI-linac in a water phantom of simple cubic geometry for different magnetic field strengths. It was demonstrated that an external magnetic field has a negligible influence on the TDCS which justified the use of TDCS values for randomly oriented water molecules in all subsequent simulations.

The next activity focused on the implementation of the magnetic field effects in a track structure code *PTra* developed at PTB for simulating the footprints of ionizing radiation at the nanometric scale [5]. The code simulates step by step each single interaction undergone by the particles traversing the medium; in our case electrons of energy lower than 1 keV. For this purpose it transports each electron to the next interaction point. The first modification applied to *PTra* was to model the influence of an external *B*-field during the transport of each electron by means of the Lorentz force. The second modification consisted of the consideration of the water molecule orientation in the DCS for ionization. In the ionization process the impact of the incoming electron on a water molecule leads to the scattering of the incoming electron and the emission of a secondary electron. It was found that the orientation of the water molecules influences the energy and direction of the emitted electron. The computed ionization DCS represents too large an amount of data to be efficiently implemented in *PTra*. Therefore this information was condensed for each primary electron energy and ionized molecular shell in the form of variances of the electron production cross sections, covariance matrices relating the energy of the secondary electrons to its emission angle, and covariance matrices relating the emission angle to the scattering angle. These matrices were then used to generate cumulative probability distributions necessary for the random sampling of the new kinematic parameters of the electron after interaction with the oriented water molecule.

The characterization of particle track structure in nanodosimetry is based on the formation of ionization clusters within a specified cylindrical volume of matter, which is generally chosen to be comparable in geometry and mass per unit area to a short segment of DNA. The number of ionizations produced by a

passing particle track within the volume is referred to as the ionization cluster size (ICS). For a large number of particles (stochastic of nature) a distribution of ionization cluster sizes (ICSD) is obtained. The cumulative probability, F2, of getting more than two ionizations within the target volume can be related to the probability of inducing a DNA double strand break (DSB), and hence to the relative biological effectiveness (RBE) of the studied radiation [6]. The aim of this activity was to determine the influence of an external magnetic field on the ICSD for several therapeutic radiation beams. For this purpose the secondary electron spectra of selected radiation types with and without external *B*-field of 1.5 T were needed as an input for the track structure simulations. These spectra were determined in a cubic water phantom for four different mono-energetic radiation beams (^{60}Co photons, 6 MV photons, 5 MeV electrons and 15 MeV electrons) using the condensed-history Monte Carlo radiation transport code GEANT4 [8]. The spectra were then fed as an input into a previously developed augmented version of PTra in order to determine the ICSD characterizing the track structure of a specific radiation beam. The consortium found that the ICSD of all four considered radiation beams are similar. Moreover the application of a static magnetic field of 1.5 T did not change the ICSD as the elastic mean free path of the secondary electrons is smaller than the radius of curvature of the electron trajectory due to the Lorentz force (Fig. 3.5-3).

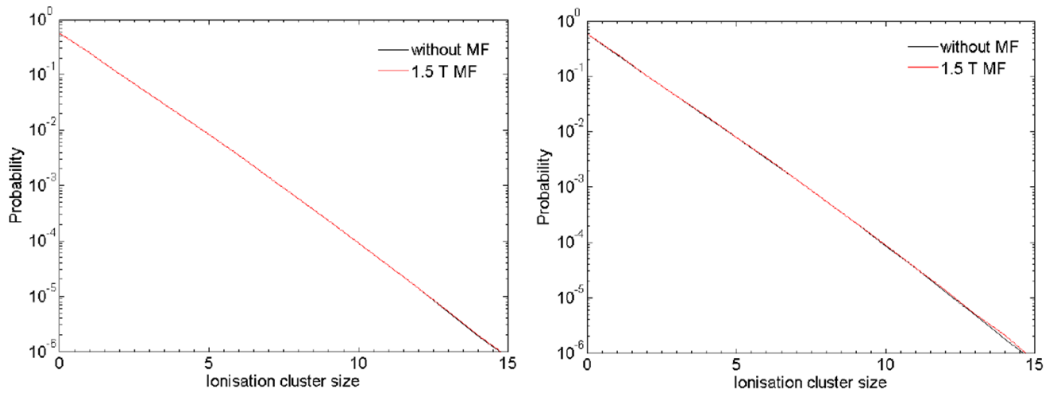

Fig. 3.5-3 *Ionization cluster size distributions for 6 MV photons (left)and 15 MeV electrons (right) obtained without and with a static magnetic field of 1.5 T. The magnetic field effect is negligible as the two curves within each graph are virtually indistinguishable.*

Another aim was to investigate the potential influence of strong external *B*-fields on the track structure and hence on the RBE of secondary electrons produced by therapy radiation beams in a water phantom. The RBE with respect to the formation of DSBs with and without applied *B*-field was assessed using a combinatorial approach proposed by Garty et al. [7]. This approach predicts the frequency distribution of DNA strand breaks based on the knowledge of the ICSD and on an empirical parameter describing the probability for an ionization to be converted into a strand break. Using the ICSD simulated within the project and the model of Garty et al., the probabilities P(DSB) to obtain a DSB were calculated for all radiation qualities of interest, with and without magnetic field. The changes in the values of P(DSB) observed with and without magnetic field were found to be well within the statistical uncertainties of the track structure simulations. Hence, using a RBE equal to unity with respect to DSB formation is reasonable for all investigated radiation qualities.

3.5.3 Key results and conclusions

- An MRI compatible, transportable absorbed dose to water primary standard was produced and commissioned in conventional ^{60}Co and MV-photon beams.
- A benchmarking method for dose simulations in Monte-Carlo codes in the presence of a *B*-field was developed as a key value to the modelling and application of detectors in MRI-accelerators.
- For a subject in an MRI-accelerator, the relative biological effectiveness of radiation could, in principle, be modified by the presence of a magnetic field. Knowledge and understanding of such effects is a necessary prerequisite of any dosimetry concept and several potential mechanisms were investigated in detail:

- Computations showed that the *scattering* of an individual secondary electron by a water molecule is not noticeably affected by the *B* field but processes involving *ionisation* do depend on *B*.
- An existing Monte Carlo code to model the track structure of secondary electrons in water was extended to include magnetic field effects, i.e. the Lorentz force and the ionisation effects just mentioned.
- Finally it was investigated whether the aforementioned effects of an external B field on the track of a single secondary electron result in a detectable *cumulative* effect on the number of DNA double strand breaks induced by single 6 MV or 15 MV photon and the result was that no cumulative effects were detectable. The project thus established that the Relative Biological Effectiveness of photons for radiation therapy are not affected by the magnetic field of an MRI scanner.

References 3.5

[1] Salvat et al., OECD NEA Data Bank/NSC DOC 2011
[2] de Prez et al., in preparation
[3] Burns et al. 2015 Draft B, Metrologia
[4] J.A de Pooter, L.A. de Prez, H. Bouchard, accepted by Phys. Med. Biol. 2015, PMB-102149
[5] Bug et al., Radiat. Phys. Chem. 81, 1804-1812 (2012).
[6] Grosswendt, Radiat. Prot. Dosim. 115, 1-9 (2005).
[7] Allison et al., IEEE Transactions on Nuclear Science 53, 270-278 (2006).
[8] Garty et al., Phys. Med. Biol. 55, 761 (2010)

3.6 Metallic implants in MRI

The bulk of the work addressing objective 6 on metallic implants in MRI only occurred in the final year of the project. This is a necessary consequence of the fact that most of the foundations for this work had previously to be developed within the project while addressing objectives 1 and 2. The scope of this part of the project was thus limited to some first, principle results on implant related aspects of MRI Safety. Also it was clear that a clear line separating method development (objectives 1 and 2) from application (objective 6) cannot be drawn. Three groups from London (KCL), Berlin (PTB), and Turin (INRIM) participated in this work. In a way this just continues and extends the story told in subsection 3.2, only with KCL taking the lead now. The master theme of the MRI Safety project, a workflow from one partner to the other, a partial sharing of the workload by parallel processing in different groups, continued and in way culminated in the work for objective 6. This close cooperation enabled (and required) more than just one partner to extend their capabilities; it also proved most helpful when dealing with critical delays as it allowed for flexible responses and an efficient risk management.

3.6.1 Development of anatomical voxel models carrying implants

To account for implants, the anatomically realistic voxel models of both adult males (Duke and Norman) and females (Ella and Naomi) were modified such that a set of voxels representing a generic hip prosthesis (Fig 3.6-1a) was inserted in an anatomically appropriate manner. Initially a simple prosthesis consisting of an acetabular head, mid-section and shaft was used and implanted bilaterally. This represented a cemented stem CoCrMo (ASTM F75 alloy) hip prosthesis with a 150 mm long stem and a hemispherical head of diameter 28 mm. In this report we refer to these prostheses as ‘bilateral implant’.

3.6.2 Exposure of patients with hip-prostheses

Exposure of patients with hip-prostheses undergoing MRI diagnosis was investigated by adopting the EM and thermal models previously described. The aim was to estimate energy deposition and temperature elevation in the metallic implants and in the surrounding tissues. Moreover, the potential use of external field monitoring was investigated to estimate the effects within the body caused by the presence of implants, and to correlate the spatial distribution of the SAR with temperature elevation.

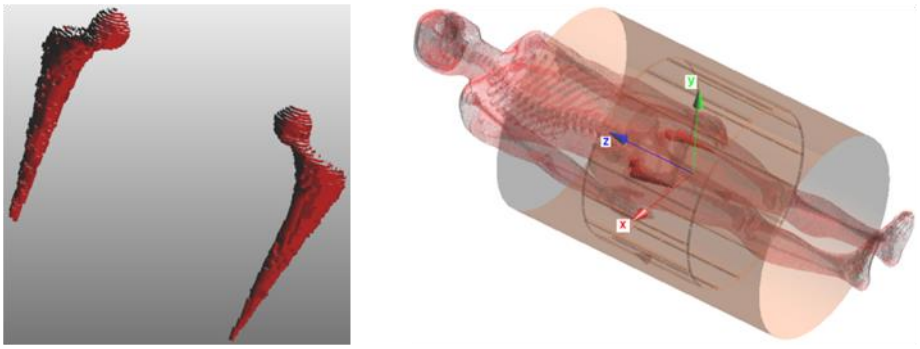

Fig. 3.6-1 *(a) Bilateral CoCrMo hip prostheses. (b) Duke model with bilateral hip prostheses in bird-cage coil.*

Both FDTD and FIT numerical approaches were used to expose these models to the simulated RF fields from a generic 16 rung shielded band pass birdcage coil tuned to 64 MHz or 128 MHz (Fig 3.6-1b). When the prostheses were immediately outside the coil, the maximum SAR_{10g} close to them was compliant with recommended limits [1]. This suggests that significant heating of the implant is unlikely for MR procedures involving patients with a CoCrMo ASTM F75 alloy hip prosthesis if the volume of interest is such that the prosthesis lies outside the birdcage body coil. On the other hand, when the prostheses are located within the birdcage body coil, caution is required, because it is likely that local enhancement of SAR_{10g} close to an extremity of the prosthesis will occur. This is particularly so when the tip of the shaft of a prosthesis is located close to the mid-(axial) plane of the coil. The local SAR_{10g} close to the prosthesis was dependent on the body model, operating frequency, and position of the prosthesis relative to the transmit coil. When normalised to whole body SAR of 2 W/kg, the maximum SAR_{10g} in the region of the implant was approximately 30 W/kg. Only a small increase in SAR_{10g} was seen close to bilateral prostheses compared to that close to a unilateral prosthesis. Results suggested that the local SAR_{10g} was highly dependent on the location of the prosthesis shaft within the femur.

Later in the project an improved hip prosthesis model was used (Prosthesis 2) that also included an acetabular shell, liner and fixing screw in simulations as a left or right hand unilateral implant. In all cases exposure to the RF field generated by a generic birdcage coil was simulated. Simulations with 12 positions of the body relative to the coil were performed and simulations involving the voxel body model without a prosthesis were executed for comparison.

Whilst most of the simulations assumed the prostheses consisted of a CoCr alloy, other variants including TiAl6V alloy, ceramic acetabular heads (of Zirconia or Alumina) and differing shaft lengths and fixing screw lengths were considered. Three different numerical methods, FDTD, FIT, and FEM/BEM, were applied to investigate the interaction of the RF fields from the birdcage coils with the voxel body models carrying implants.

Results indicated that at 64 MHz, the maximum SAR_{10g} occurred close to either the screw of the shaft or the tip of the prosthesis when the implant was within, or partially within, the footprint of the coil. The maximum value normalised to $B_1^+ = 1$ µT at the coil isocentre was 1.3 W/kg. At 128 MHz, the SAR_{10g} values (normalised in the same manner) close to the prosthesis were higher, ranging from approximately 3 to 6 W/kg.

The results from the simulations in which the prosthesis was assumed to comprise of different materials were dependent on the relative position of the coil and prosthesis. In some cases the local SAR_{10g} close to the prosthesis was greater for the CoCr prosthesis than for the one with a ceramic acetabular ball whilst in other cases the converse was true. Since both CoCr and TiAl6V are both relatively highly conductive, the numerical methods used approximated them as being perfectly electric conductors and so were unable to differentiate between these alloys.

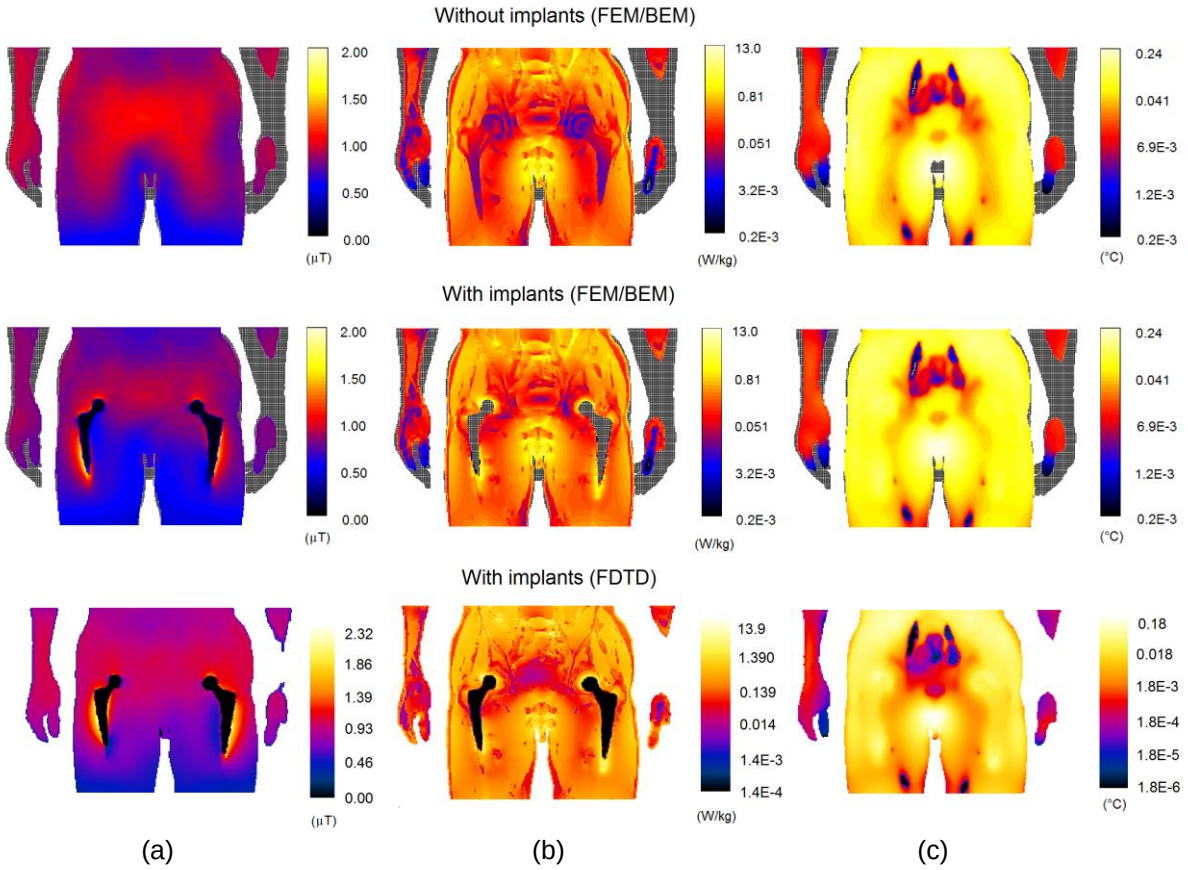

Fig. 3.6-2 *Maps of B_1^+ (a), local SAR (b) and temperature elevation (c) in the coronal section obtained at 128 MHz with FEM/BEM (intermediate row) and SEMCAD-X (bottom row). The maps computed with FEM/BEM in absence of the implants are displayed in the top row. Numerical values on the chromatic scales are, respectively, in tesla, watt per kilogram, and degrees Celsius.*

The FEM-BEM approach was applied to simulate exposure of Duke with the bilateral implant in several axial positions with respect to the bird-cage coil isocenter, and the spatial distributions of *B*-field, local SAR and steady-state temperature elevation were determined for each case. These results were compared to those obtained using FDTD. An example of the effect (at 128 MHz) of the bilateral implant on the spatial distribution of B_1^+, local SAR (not averaged) and temperature elevation in a coronal section of the pelvic region is shown in Fig. 3.6-2. Comparisons of B_1^+ spatial distributions in the coronal sections show evidence of the “shielding effect” of the metallic implant, due to induced currents strongly localized near the material surface which cause a concentration of magnetic flux density peak values in tissues located in close proximity to the prosthesis tips and legs. The field is essentially unperturbed at a small distance. Maximum values of local SAR (99th percentile) and temperature elevation in the prostheses and surrounding tissues are summarized in Table 3.6-I.

Both methods showed an approximately twofold enhancement of B_1^+ close to the prostheses at 128 MHz compared to the body model without prostheses. At 64 MHz an enhancement of up to 50 % was found. These changes in magnetic flux density are highly localised around the prostheses. Non-spatially averaged local SAR hot spots close to the prosthesis extremities were predicted, with maximum values obtained by the two methods agreeing within about 7 %. Compared to the native state, the introduction of the implant induces large increases in (not spatially averaged) local SAR, in particular at its extremities (tip and ball end). However, similar absolute values of local SAR were found in other tissues of the pelvis, uncorrelated to the implant. Our results clearly indicate that the presence of the implant can cause an increase of local SAR in certain tissues (e.g. bone). Simultaneously, however, local SAR can be reduced in other regions or tissues (e.g. fat and muscle). The major result of the thermal simulations is the observation that local SAR and temperature elevation are only weakly correlated, also true in the presence of the implant, due to the effect of the blood perfusion.

Table 3.6-I. *Summary of results for SAR (without spatial averaging) and temperature elevation with and without hip implant*

TISSUE	With hip prosthesis		Without hip prosthesis	
	Local SAR (W/kg)	Temperature elevation (°C)	Local SAR (W/kg)	Temperature elevation (°C)
Bone	1.05	0.50	0.64	0.56
Fat	1.47	0.83	1.80	0.93
Marrow red	2.18	0.41	0.59	0.46
Muscle	1.61	0.77	1.95	0.86
Prosthesis	-	0.41	-	-

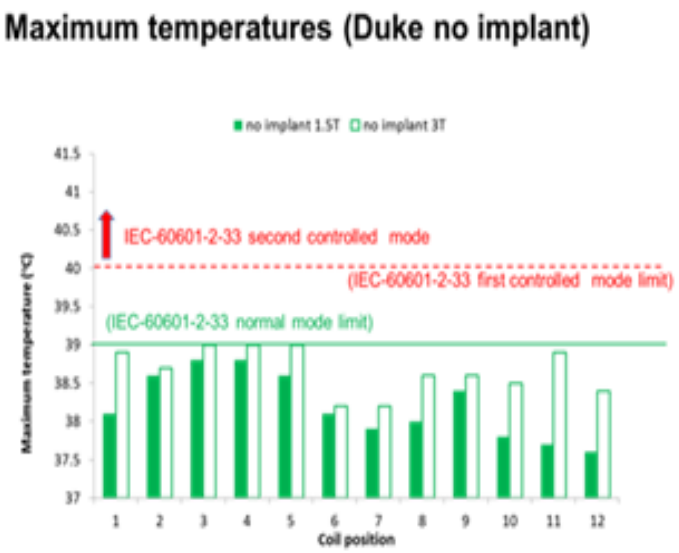

Fig. 3.6-3 *Maximum temperatures resulting from 600s RF exposure (SAR10g,max = 10 W/kg) for the Duke model.*

When comparing surface B_1^+ and B_1^- field values with and without prostheses; higher values were detected in the region of the thighs and hips in the absence of prostheses. Changes in the surface electric field were small or non-existent. Although there are some correlations between the surface B_1 field and the presence of large metallic implants, the conclusion drawn is that monitoring of internal effects from external field measurements would be difficult and not sufficiently reliable for practical purposes, particularly in view of patient to patient variability.

This study on the RF field interaction with hip prostheses and its dependence upon the relative position of the subject and body coil and prosthesis composition together with resulting tissue temperature changes shows significant findings. It will extend knowledge and hence will contribute to safe clinical procedures involving this large population of patients. One of the major goals of this JRP was to explore the viability of MRI safety concepts that use external field probes close to the patient to detect potentially hazardous 'anomalies', in particular the presence of metallic implants. While this scientific goal was indeed achieved, the result was, unfortunately, not the desired one. The effects of internal implants on

the external EM field distributions appear to be too small to allow for a robust detection and utilization within a safety concept, at least for the practically most relevant case of the birdcage body coil as the RF transmitter.

Additional thermal modelling was carried out using the FDTD solver bioheat transfer equation within SEMCAD v14.8.6. Thermal properties of tissues were, once again, taken from the IT'IS database. The ambient temperature was assumed to be 25 °C and the heat transfer coefficient between skin and air was taken to be 10.5 W $m^{-2}K^{-1}$. The temporal sequence of all thermal simulations was as follows: RF power was off during the period t = 0 to t = 1500 s (to allow a baseline temperature distribution to be achieved), and was on from t = 1500 s to t = 2100 s. RF power was normalised such that the maximum local SAR_{10g} within the trunk (SAR_{10g} trunk) predicted in the corresponding electromagnetic simulation was 10 W/kg. The spatial distribution of temperature was recorded at 60 s intervals during the RF-on period and value and location of the maximum temperature at t = 2100 s were determined.

For both 1.5 T and 3 T without implant, $T_{max} \leq 39$°C following 600s RF with $SAR_{10g,max}$ = 10 W/kg, suggesting compliance with IEC-60601-2-33 normal model operation. Only for the coil approximately heart-centred or approximately knee-centred was $T_{max} < 39$°C when a prosthesis was present. In six positions, $T_{max} > 40$°C and the maximum temperature occurred at shaft or screw tip for eight of the implanted models. These results suggest that in most cases for which the prosthesis is within the coil footprint, operation under IEC-60601-2-33 second controlled level conditions would be required. Some spatial correlation between maximum SAR_{10g} and maximum temperature was seen for worst case and near worst case positions of the body/prosthesis relative to the coil, although such correlation was poorer for other positions. Recently it has been suggested that thermal dose (i.e. a combination of elevated temperature and its duration) with units of equivalent minutes at 43°C could be a useful parameter in assessing safety [2]. In the simulations described above, the thermal dose is estimated to be up to 2 CEM43°C following 600 s of RF heating at a maximum SAR_{10g} = 10 W/kg, a value suggested as being safe for patients with compromised thermoregulation imaged under controlled conditions.

3.6.3 Gradient effects

Going beyond the original objective 6, the work was extended to consider the heating effects of switched gradients on hip prostheses. The reason to do that was mostly scientific curiosity. As all the necessary modelling ingredients for such an investigation had already been developed within the project and were available, it was tempting to combine and apply them. It is commonly believed in the MRI community that gradient heating effects on metallic implants are negligibly small and the simple goal of the present work was to test this hypothesis. The two types of prosthesis described above were used as examples and three sets of gradient coils were considered (Fig. 3.6-4): i) a conventional system suitable for cylindrical MRI scanners (the magnitude of the gradient and the diameter spherical volume, DSV, were 30 mT/m and 500 mm, respectively); ii) a set designed to be used inside MRI-LINAC platforms for which each axis is equipped with a pair of separated coils ('split coils'), providing a central gap for use during LINAC treatments (the gradient coils produce a gradient of 30 mT/m within a 300 mm DSV); iii) a set of uniplanar coils, specifically used for scanning the spinal cord (a 50 mT/m gradient is produced in a small region around the spine). All sets include x-, y-, and z-coils, fed with a current with a main harmonic of 1 kHz.

The hybrid FEM-BEM method was used for this purpose because, unlike FDTD or FIT, it is also applicable at kilohertz frequencies. The results show that the power deposition due to the EM field is confined inside the metallic implant, i.e. power deposition inside human tissues with their finite electrical conductivity is negligible in the given frequency regime. The non-negligible power deposition in the implant itself is then used in a thermal simulation to estimate the resulting state temperature. All coils were assumed to be energised simultaneously and in phase and INRIM's FEM Pennes' based thermal model was used to predict temperature changes in the tissue. A train of trapezoidal gradient pulses, symmetric with respect to zero, was considered. The frequency of one complete trapezoidal wave (including a positive and a negative half-wave) was 1 kHz; harmonics up to 7 kHz were also accounted for. This waveform was repeated N times during an interval t_{on} and then the coils were switched-off for a time t_{off}. This sequence was repeated periodically during the MRI scan. The results obtained for the unilateral implant are qualitatively similar compared to the ones for the bilateral implant, but smaller in magnitude (due to the features of the single prostheses, not because of their number). CoCrMo prostheses resulted in temperature changes approximately 1.5 – 2 times higher than TiAl6V prostheses, and therefore represented the worst case. Results suggest an increase in the temperature close to a prosthesis of up to 3-

4 °C depending upon the coil geometry. Results obtained with the axial arrangement of split coils and in the radial arrangement with one side facing the floor are qualitatively similar to those found with conventional gradient coils. However, the worst case is predicted to occur when the back is facing the floor in the radial arrangement. These results shatter the widespread assumption that heating effects due to switched gradients are generally negligible. The findings indicate a possible concern for safety and certainly call for additional experimental and numerical investigations [3].

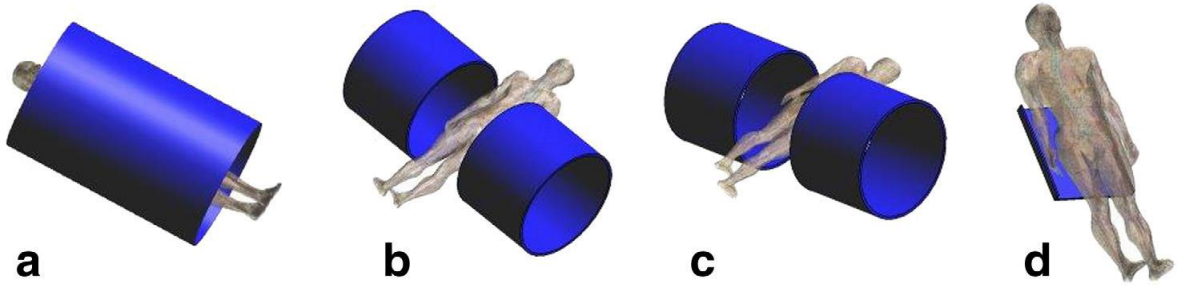

Fig. 3.6-4 *Gradient coil sets: a) conventional coils, b) and c) split coils, d) uniplanar spinal coil*

3.6.4 Exposure of patients with metallic wires

The effects induced within and in close proximity of a metallic wire exposed to the RF field of a birdcage coil were investigated to estimate the spatial distributions of *E*- and *B*-fields and local SAR. A generic deep brain stimulation (DBS) electrode and lead implanted into the brain of a female child was considered. Since some dimensions of the DBS electrode and lead are small (≤ 1 mm), typically determined by the thickness of insulation or the pitch of a helical lead, this presents a challenge when segmenting the model into voxels. The contrast between the dimensions of the wire and those of the head prevent a direct, simultaneous simulation of head and wire on accessible computing hardware. Since the effects are known to be local to the electrode and lead, a Huygens box approach in which the head without electrode/lead is simulated and the fields evaluated at the surface of a local box around the implant are used as the source for a second simulation of this smaller volume but at a resolution compatible with the wire dimensions.

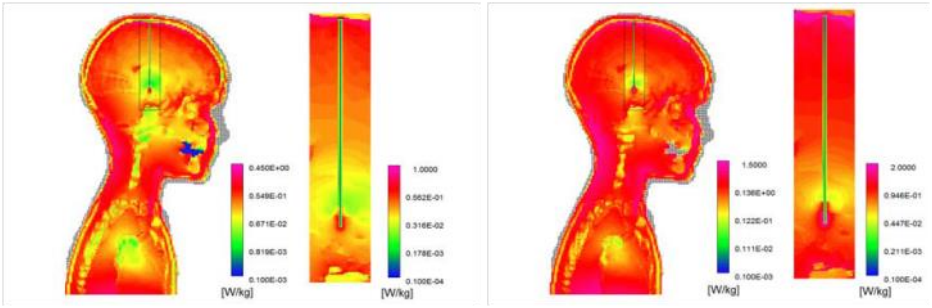

Fig. 3.6-5 *Sagittal sections showing SAR for 64 MHz exposure (left) and 128 MHz exposure*

INRIM investigated the effect of varying the dimensions of the box and of the voxels within it (0.2 mm and 0.4 mm) for a straight wire (Fig. 3.6-5) and found that (i) the effect of the wire is highly concentrated in close proximity to the wire tip and does not extend to a larger area; (ii) the temperature increases near the wire tip are comparable with those obtained in tissues far from the wire in absence of the wire; (iii) the results obtained with the different models are not completely equivalent at the very local level. Further work is required to completely resolve this problem; within the time constraints of the current project only preliminary investigations could be concluded.

Simulations were carried out at 64 MHz and 128 MHz for four positions of the head relative to the isocentre of the coil (Fig 3.6-6b) and at 300 MHz for one of these positions. Increasing the frequency resulted in an increase of SAR at the tip of the electrode (~20 fold at 128 MHz and ~180 fold at 300 MHz relative to 64 MHz) and to a greater change of local temperature (~7-8 fold at 128 MHz and ~80-100 fold at 300 MHz relative to 64 MHz).

At KCL similar simulations were carried out at 128 MHz using a SEMCAD solver with the Huygens box approach. The head was positioned in the birdcage coil such that the thalamus was isocentred (Fig. 3.6-6a). The tip of the DBS electrode was in the globus pallidus. Increasing the impedance of the electrode lead, by introducing series connected lumped inductors in a 160 cm lead, significantly decreased *E*-fields and SAR around the electrode tip compared to a simple Pt/Ir lead, but locally high *E*-field and SAR were introduced around each lumped inductor. However, this approach may be a viable solution if a larger number of discrete inductors are introduced into the lead. Increasing the resistivity of the lead material to provide ~30 kΩ resistance along the lead resulted in a reduction in the maximum *E*-field at the tip by a factor of approximately 70 and local SAR_{1g} by a factor of 1.4 compared to the case of a (low loss) Pt/Ir lead. However, in both cases the maximum SAR_{1g} occurred in the CSF close to the entry of the lead through the skull; the 30 kΩ lead reduced this by a factor of approximately 2 compared to the Pt/Ir lead.

Initial simulations of the case of a generic DBS electrode and lead implanted into the head of the Roberta female child model, predicted that the largest increase in temperature close to the lead/electrode occurred at the interface between skull and CSF. In the case of 600 s of 128 MHz exposure and a Pt/Ir (sheathed) lead, the temperature increase resulting from FDTD computed SAR values was ~0.07 °C (normalised to $B_{1,rms}$ of 1 µT at the isocentre) and ~0.03 °C at the electrode tip. Introducing 30 kΩ impedance into the lead reduced these values by a factor of ~50 at the electrode tip and ~3 where the lead passed through the skull/CSF interface. Transient behaviour suggested that temperatures reached steady state in approximately 400s.

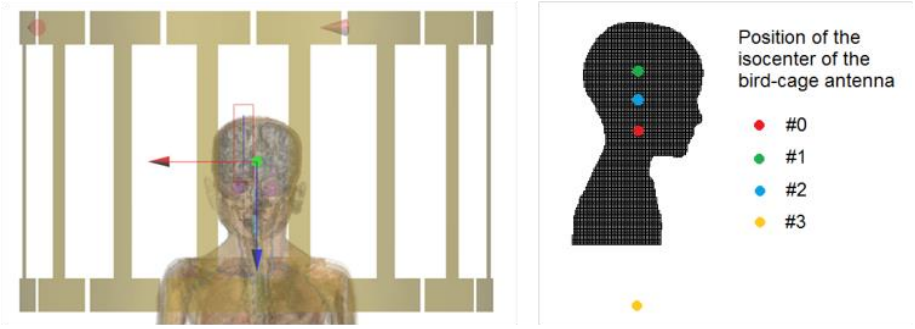

Fig. 3.6-6 *(a) Roberta model with DBS electrode lead within birdcage coil used in FDTD simulations. The Huygens box is shown in red. (b) positions of birdcage coil isocentre relative to head used in simulations performed by INRIM.*

Calculations performed at INRIM also predicted that the maximum temperature increase along the lead occurred close to the skull/CSF interface with a secondary maximum at the electrode tip. However, these calculations were performed using a different position of the head relative to the birdcage coil (position 0 in Fig. 3.6-6b) and different thickness of insulation along the lead than assumed in the FDTD simulations outlined above. At all of the frequencies considered (64, 128 and 300 MHz), the temperature increases near the wire tip were comparable with those obtained in tissues far from the wire, in absence of the wire. The predicted local temperature increases at steady-state (normalised to B_1^+ = 1 µT at the iso-centre) and close to the wire tip were 0.0005 °C (64 MHz), 0.005 °C (128 MHz) and 0.05 °C (300MHz). In these cases, transient behaviour suggested that steady state temperatures were achieved after approximately 500 s.

3.6.5 In-situ measurements of RF currents in implanted wires

PTB developed an RF current sensor based on a Rogowski coil with fibre optic readout for the measurement of induced currents in the protruding end of wire type implants inside an MR scanner as shown in Fig. 3.6-7.

The ASTM phantom was implanted with a fine wire that was bent through 90 degrees near the exit from the phantom. Two cases – one with the wire in the 'shoulder' region and one with the wire in the 'head' region – were considered. A schematic representation of the positioning of the wire (left hand) and the actual set up (wire in shoulder), including the location of the RF current sensor (right hand) are shown in Fig. 3.6-7.

Both the measurements on implanted wires in the 'shoulder' and the 'head' section of the body phantom revealed substantial currents (up to 100 mA at 1 kW input power to the body coil of the MR scanner) even when the complete wire and the larger part of the phantom itself were already well outside the RF coil.

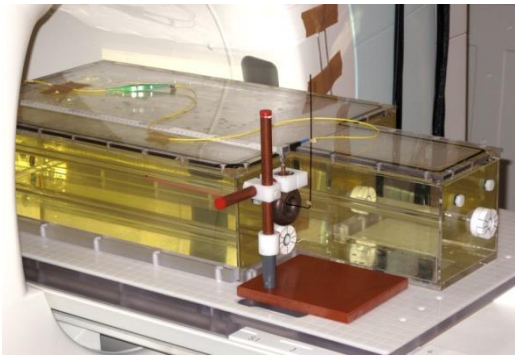

Fig. 3.6-7 *Photograph of the ASTM phantom with wire implant and current sensor.*

The experimental setup was also modelled using FDTD and the results compared with the experimental data. In the case of the wire in the shoulder region (which resulted in a larger current on the wire than in the case of the wire in the head), the peak current detected in the wire was 360 mA; when the centre of the phantom was located at the coil isocentre, the measured current was 130 mA. From the results of the simulated current density profile along the wire shown in Fig. 3.6-8, corresponding current of ~150 mA is obtained. Since the simulations were done on a relatively coarse grid and not aiming at truly quantitative results this is considered a satisfactory agreement.

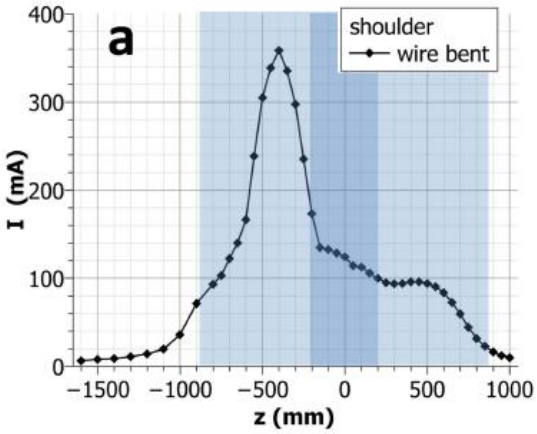

Fig. 3.6-8 *Measured current on wire, z is the position of the centre. The light and dark blue shading indicates the extension of the RF transmit coil and the MRI magnet, respectively.*

3.6.6 Summary implants

- A concept was developed to qualify different positions of an implant carrying patient in the MRI scanner's RF coil as safe or critical. By a series of numerical simulations for an exemplary implant type, a hip prostheses, critical patient positions in the scanner were identified where tissue temperatures could exceed the permissible limit of 39 °C. Practically also highly relevant is the fact that regimes of safe positions could be stated where no noticeable effects of the implant are detectable and implant carriers can safely be scanned.
- Another important finding was the observation that tremendous simulation errors can result when a hip prosthesis is not accurately orientated within the computer model of a patient. In particular for long implants such alignment faults can easily occur. This hints at a principle limitation of present modelling approaches.

- In an extension of the original research program, tissue heating effects due to an MRI scanner's switched gradient fields were also investigated. The simulation results are alarming as they show that temperature rises of up to 3-4 °C can occur close to the implant. This raises serious concerns and calls for further investigations of this hitherto completely neglected aspect of MR safety.
- An approach was tested to reduce the danger associated with wire-like implants. A simplified model of a deep brain stimulator electrode was investigated and it was found that the local SAR at a critical point near the skull can be significantly reduced by using a high-impedance lead. This mitigation approach is helpful, therefore, but not sufficient since an alarming temperature increase of several degrees Celsius can still occur inside the brain, at the electrode tip.
- An MRI compatible sensor to measure RF currents induced in implanted electrodes was engineered and tested. Phantom measurements with this sensor were in good agreement with corresponding simulations. This indicates that such a sensor can serve two different purposes: for *risk assessment*, as it provides an independent and sensitive means to test the validity of simulation results; and for *risk management*, as it can serve as a watch-dog device to detect a critical situation during an MRI scan of a patient with implant.

References 3.6

[1] IEC-60601-2-33
[2] Van Rhoon et al., Eur. Radiol. 23, 2215-27, 2013.
[3] L. Zilberti, O. Bottauscio, M. Chiampi, J. Hand, H. Sanchez Lopez, R. Brühl, and S. Crozier. Magn Reson Med 2015. doi: 10.1002/mrm.25687

4 Actual and potential impact

4.1 Dissemination

4.1.1 Publications and presentations

Already within its lifetime the partners of the MRI Safety project sought very actively to get their research results published and hence known to the community. Until the end of the project a total of 61 publications had been submitted, 59 of them published, one accepted and waiting for publication and one still under review. 25 of these 61 publications are regular papers in peer reviewed scientific journals, three are master theses and the remaining 33 are conference proceedings. The latter are also peer reviewed and publicly accessible, albeit often only after an embargo period. It is quite clear that a number of additional publications on project results will be written and submitted after the formal end of the research project. Only 14 of those publications originated out of a single group of project partners while a majority of 45 papers were published together with co-authors from academia and/or industry.

Based on project results a total of 67 presentations were given at scientific conferences, 53 of them for an international audience. Oral (33) and poster (34) presentations were equally frequent. An additional twelve project related presentations have already been accepted for international conferences in 2015 but after the formal project end; more will certainly come. In the vast majority of cases the presentations were addressing predominantly the scientific community; occasionally a mixed audience, typically including representatives from industry, public bodies or agencies, or the general public were addressed. Among conference presentations the share of authorships from a single partner group was higher compared to publications but still a number of 30 contributions were joint presentations with co-authors from academia. In addition to these 67 conference contributions another 14 presentations of project results were given at smaller events like workshops or seminars.

4.1.2 Training, workshops, stakeholder meetings

Partners of the MRI Safety project have been engaged in a number of training activities. Two of them were addressing other partners within the consortium, one organised as a satellite event to an international MRI conference, the other a one-to-one training of a mobility-grant researcher during his three-months stay at the academic project partner. Another eight training courses or lectures from project scientists were targeting a general scientific audience, however. INRIM was regularly involved in a training course on Mathematical-Physical Aspects of Electromagnetism and in a training course on Electromagnetic dosimetry in MRI for PhD students from Politecnico de Torino; PTB scientists and engineers

were giving hands-on training in RF coil building and characterisation at annual workshops, endorsed by ESMRMB, the largest professional society for MRI in Europe, at the Berlin Ultrahigh Field Society.

'Open Lab Days', 'Science Nights', and similar events are popular occasions for scientists to explain their work to the general public. Four times within the project's duration consortium members seized such an opportunity and included goals and results of the MRI Safety projects into their presentations and guided lab tours.

The consortium partners were not content to present their results at numerous established conferences (see 4.3.1), in addition they also engaged in organising (or co-organising) a number of events for themselves. This included international conferences with hundreds of attendees but most of them were smaller events like seminars or workshops with a well-defined focus on project topics targeting a specifically interested audience. In total twelve such events were (co-)organised by consortium members within the three years of the project's duration.

Stakeholder needs were the initial trigger for the MRI Safety project and close interaction with stakeholders accompanied the project from its beginning to the end. Six out of six project meetings were also stakeholder meetings, attended by stakeholders and actively shaped by their contributions and questions. In addition to the aforementioned workshop organisations, which always implied stakeholder interaction, 23 meetings with stakeholders, often from industry, were held to discuss specific, project related subjects.

4.1.3 Standardisation bodies

Consortium partners were active in four different standardisation bodies. PTB is represented on the IEC62B-MT40 working group within the TC 62B technical committee and also on its national mirror in Germany, the NA 080-00-08 AA / NA080-00 18GA. These working groups are concerned about all aspects of MRI, with safety being one major topic. During the project lifetime six committee meetings took place and PTB actively participated in all of them. A presentation on the MRI Safety project, its goals and first results had been explicitly on the agenda of one national and one international board meeting.

Nine times over the project duration consortium members from VSL were contributing to the regular board meetings of the Nederlandse Commissie voor Stralingsdosimetrie (NCS), a bi-national Dutch/Belgium standardisation body for radiation dosimetry. This board was also informed about the EMRP project on MRI Safety by a dedicated presentation during one of the meetings.

Project scientists from INRIM are active on the CEI – TC 106 committee on human exposure to electromagnetic fields, the Italian mirror to the IEC TC 106 technical committee. They presented the project activities on two different board meetings.

4.2 Early Impact

It will take years before the full impact of the MRI Safety project is achieved and can be assessed. Nevertheless, there is some 'early impact' which can already be reported.

- Representatives from Elekta, leading European manufacturer of radiotherapy equipment, confirmed in March 2013 that "*... The EMRP project HLT06 contributes exact and reliable radiation dosimetry to this endeavor, an indispensable precondition before any patient can be treated. Thanks to EMRP results manufacturers Elekta were in the position to make the next step...*" i.e. bring the system to the market.
- Project partners from Turin developed a new formulation to calculate motion induced electromagnetic fields in the human body. Australian colleagues recognized the value of that approach and a fruitful cooperation emerged, resulting in three journal papers and two conference proceedings, so far.
- Scientists from the Berlin Ultrahigh Field Facility expressed interest in the methodology developed for metallic implants in MRI. In collaboration with the consortium they used the simulation methodology and equipment developed in the project to systematically investigate and validate the potential safety hazards of cardiac stents in MRI, resulting in one journal publication and three conference proceedings.

- Representatives from *Bundesamt für Strahlenschutz*, the German authority for radiation protection, and ICNIRP closely followed and interacted with the project from the start. Findings from the motion-induced field work affected certain statements in the guidelines. But the most important effect of the collaboration, according to an ICNIRP expert, was the fact that it helped them to sharpen their view and get confidence in their physical picture of the problem, thus supporting them in devising their new guidelines (Health Phys. 106, 2014, 415-25). Vice versa, project scientists benefitted a lot from these intense discussions and the publication of the guidelines affected further project activities in that field.

In addition, some recent developments can be reported which were not *caused*, but supported by the MRI Safety project.

- In 2015 the 2nd amendment to the IEC-60601-2-33 was voted upon and unanimously accepted. This amendment will allow, for the first time, CE marking of 7T MRI scanners thus paving the way for ultrahigh field MRI into the clinical routine. The consortium was represented on the maintenance team for the IEC standard and also on one national mirror committee which was voting on the new amendment.
- Shortly after, leading European MRI manufacturer Siemens announced their decision to actually take that step and to develop the first *clinical* (CE marked) 7T scanner, thus making this high-end technology finally available for patients.
- For 2015, the German Research Foundation (DFG), launched two funding programmes centred on MR guided radiotherapy. This documents high expectations and confidence in such new technology.

4.3 Addressing end user needs

In its 2011 Research Agenda the World Health Organisation (WHO) stated a number of “high priority research needs" with respect to EMF dosimetry (i.e. including MRIs) for example to "*assess characteristic RF EMF emissions, exposure scenarios and corresponding exposure levels for new and emerging RF technologies and for changes in the use of established technologies: This work should address the latest developments in areas such as ... body imaging*". This request was successfully addressed as the project made a number of significant dosimetric contributions addressing the specific case of MRI. Methods were developed to assess characteristic MRI related RF emissions in general and in particular for emerging technologies/changes in use of existing technologies like ultrahigh fields (e.g. 7T MRI scanners) and pTx.

The latter two technologies are innovative developments in MRI but pose new safety hazards. Project results show that these hazards can be successfully contained, which helps not only to protect EU citizens but also supports the technology leading EU manufacturers in bringing these innovations into the clinical routine.

Almost 10 % of the European population are carrying medical implants but no clear metric existed to assess this safety hazard in MRI. To develop such a metric is a long-term task but a few first steps in this direction were achieved within the project. The investigation of exemplary implant types with numerical simulations and the development of sensors capable to measure potentially hazardous induced currents in wire-like implants are relevant contributions to the development of such a metric.

The 2004/40/EC directive was aimed at health and well-being of employees but unintentionally almost banned MRI as it was argued that exposure limits were already exceeded when a worker approaches the scanner. The project addressed this problem by providing the proper numerical techniques to quantify the exposure in terms of induced electric fields and current densities inside the body. It was shown that it is indeed possible to exceed the limits as given in the most recent guidelines. It is now up to legislators to draw conclusions on these findings as only unpleasant, temporary sensations but no truly adverse health effects result if the guideline limits are exceeded.

MRI-accelerator combinations are an exciting new development with the potential to revolutionize radiotherapy of cancer. However, no traceable dosimetry existed for this application but is a required precondition before patients can be treated. The project provided such traceable dosimetry and was of utmost

importance, therefore, for large European MedTech companies pursuing the development of the MRI-accelerator.

4.4 Wider and longer-term impact

Key elements of an anticipated long term impact of the EMRP project on MRI Safety are:

- An accepted methodology will exist to assess RF and switched gradient related safety issues based on validated numerical simulations. MRI manufacturers will have implemented such simulation based safety concepts into their complete MRI product lines, not just for (current) high-end products like 7T-MRI or pTx systems. This will result in a general, sustainable lowering of the 'innovation threshold' in MRI, as a flexible and versatile safety concept which can easily be adapted to all kind of new developments is already in place. Manufacturers, including small companies supplying components and accessories, will benefit from shorter innovation cycles; patients and health care systems will both benefit from improved diagnosis and therapy control.
- Project results on the safety of metallic implants developed will contribute to the further development of the ISO/TS 10974 technical specification and help to finally convert this 'preliminary' document an into a true international standard. This will make MRI accessible to millions of hitherto excluded European citizens and will be the basis for a plethora of new implant developments by the EU MedTech industry.
- Solving the dosimetry problem was one key requirement before the MRI-accelerator can be used for patient treatment. Once this is solved, the first prototype systems can be brought into clinical trials. This development has the potential to revolutionise external-beam radiotherapy (EBRT) for cancer treatment. While primarily developed to make new tumour types, i.e. those in moving organs, accessible for EBRT, the evolution will not stop there. Considering that MRI is not using ionizing radiation and thus can be applied multiple times and for long runs without accumulating damage, it is quite clear that the technology, once it is in place, will always be used for on-line control of the target position, thus improving the accuracy and eliminating potential sources of error for any EBRT application. In addition, it is predictable that in the longer term the complete treatment planning workflow, which is today based on CT images, will be converted to MRI, thus ensuring perfect consistency between planning and treatment. In view of MRI's capabilities to image not just anatomy but also physiology and function (flow, perfusion, oxygenation, etc.) it is to be anticipated that methods for on-line therapy control during irradiation can and will be developed; MRgRT will most certainly create a complete new field of MRI related R&D: new sequences, new contrast agents, new accessories (e.g., special-purpose RF coils or fixation devices).

5 Website address and contact details

A public website (http://www.ptb.de/emrp/mri.html) has been opened and maintained, where a general description of the project, the main deliverables, results have been made available for end users and the general public. The website also served to keep the interested public informed about project meetings and events.

The following people can be contacted for questions about the project:

General questions about the project	Bernd Ittermann (PTB)	bernd.ittermann@ptb.de
RF electromagnetic field measurements	Gerd Weidemann (PTB)	gerd.weidemann@ptb.de
RF electromagnetic field simulations	Oriano Bottauscio (INRIM)	o.bottauscio@inrim.it
Motion induced low-frequency fields and currents	Luca Zilberti (INRIM)	l.zilberti@inrim.it
Parallel transmission and ultrahigh fields	Frank Seifert (PTB)	frank.seifert@ptb.de
MRI-accelerator combination	Leon de Prez (VSL)	ldprez@vsl.nl

Metallic implants in MRI	Jeffrey Hand (KCL)	jeffrey.hand@kcl.ac.uk

6 List of publications

Results of the MRI Safety project have led or contributed to the following list of peer-reviewed journal publications. Only papers which were published or accepted for publication during the lifetime of the project are included here, a number of additional manuscripts is still under preparation.

[1] *Calibration of fibre optic RF E/H-field probes using a magnetic resonance (MR) compatible TEM cell and dedicated MR measurement techniques.* T. Klepsch, T. D. Lindel, W. Hoffmann, H. Botterweck , B. Ittermann, F. Seifert. Biomed Tech 2012; 57 (Suppl.1) pp.119-122, DOI: 10.1515/bmt-2012-4428

[2] *Uncertainty Estimate Associated with the Electric Field Induced inside Human Bodies by Unknown LF Sources.* O. Bottauscio, M. Chiampi, G. Grotti, D. Giordano, W. Wang, L. Zilberti. IEEE Transactions on Instrumentation and Measurement, Vol. 62, No. 6, 2013, pp.1436-1442. DOI: 10.1109/TIM.2012.2230812

[3] *Reply to "Comments on Induction of an Electric Field in Human Bodies Moving Near MRI: An Efficient BEM Computational Procedure".* M. Chiampi, L. Zilberti. IEEE Transactions on Biomedical Engineering, Vol. 60, No. 3, 2013, pp.882-883, DOI: 10.1109/TBME.2012.2232295

[4] *Massively parallelized Boundary Element simulation of voxel-based human models exposed to MRI fields.* O. Bottauscio, L. Zilberti, M. Chiampi . IEEE Transactions on Magnetics Vol. 50, No. 2, 2014, #7025504, DOI: 10.1109/TMAG.2013.2280523

[5] *Solution of Large Complex BEM Systems Derived from High-Resolution Human Models.* G. Borzì, O. Bottauscio, L. Zilberti, M. Chiampi. IEEE Transactions on Magnetics Vol. 50 No. 2, 2014, #7012804, DOI: 10.1109/TMAG.2013.2281215

[6] *A numerical survey of motion-induced electric fields experienced by MRI operators.* L. Zilberti, M. Chiampi. Health Physics Vol. 105, No. 6, 2013, pp. 498-511, DOI: 10.1097/HP.0b013e31829b4aac

[7] *Numerical safety study of currents induced in the patient during rotations in the static field produced by a hybrid MRI-LINAC system.* A. Trakic, L. Liu, H. Sanchez Lopes, L. Zilberti, F. Liu, S. Crozier. IEEE Transactions on Biomedical Engineering Vol. 61, No. 3, 2014, pp. 784-793, DOI: 10.1109/TBME.2013.22899245

[8] *Validation of numerical methods for electromagnetic dosimetry through near-field measurements*. D. Giordano, L. Zilberti, M. Borsero, R. Forastiere, W. Wang. ACTA IMEKO Volume 4, Number 1, 90 – 96, February 2015

[9] *A Hybrid FE-BE Method for SAR estimate in Voxel Based Human Models undergoing MRI*. O. Bottauscio, M. Chiampi, L. Zilberti. Engineering Analysis with Boundary Elements Vol. 49, 2014, 15-21, DOI: 10.1016/j.enganabound.2014.04.014

[10] *Experimental Validation of MRI Dosimetric Simulations*. D. Giordano, L. Zilberti, M. Borsero, M. Chiampi, and O. Bottauscio. IEEE Transactions on Magnetics, Vol. 50, NO. 11, #5101504, November 2014. DOI: 10.1109/TMAG.2014.2323428

[11] *Collateral Thermal Effect of MRI-LINAC Gradient Coils on Metallic Hip Prostheses*. L. Zilberti, O. Bottauscio, M. Chiampi, J. Hand, H. Sanchez Lopez, and S. Crozier. IEEE Transactions on Magnetics, Vol. 50, NO. 11, #5101704, November 2014. DOI: 10.1109/TMAG.2014.2323119.

[12] *On the RF Heating of Coronary Stents at 7.0 Tesla MRI*. L. Winter, E. Oberacker, C. Ozerdem, Y. Ji, F. von Knobelsdorff-Brenkenhoff, G. Weidemann, B. Ittermann, F. Seifert, T. Niendorf. Magnetic Resonance in Medicine (2014). DOI: 10.1002/mrm.25483

[13] *A GPU Computational Code for Eddy-Current Problems in Voxel-Based Anatomy*. O. Bottauscio, M. Chiampi, J. Hand, L. Zilberti. IEEE Transactions on Magnetics. 51 (2015) 5100904. DOI 10.1109/TMAG.2014.2363140

[14] *Assessment of computational tools for MRI RF dosimetry by comparison with measurements on a laboratory phantom*. O. Bottauscio, A. M. Cassarà, J. W. Hand, D. Giordano, L. Zilberti, M. Borsero, M. Chiampi, G. Weidemann. Physics in Medicine & Biology Vol. 60, July 2015, 5655–5680. DOI: 10.1088/0031-9155/60/14/5655

[15] *Motion-Induced Fields in Magnetic Resonance Imaging: Are the Dielectric Currents Really Negligible?* Luca Zilberti, Oriano Bottauscio, and Mario Chiampi. IEEE Magnetics Letters, Vol. 6 #1500104 May 2015. DOI: 10.1109/LMAG.2015.2429641

[16] *Comparison between Simulated Decoupling Regimes for Specific Absorption Rate Prediction in Parallel Transmit MRI*. A. Beqiri, J. W. Hand, J.V. Hajnal, and S. J. Malik. Magnetic Resonance in Medicine (2014), DOI: 10.1002/mrm.25504

[17] *Specific absorption rate in neonates undergoing magnetic resonance procedures at 1.5T and 3T.* S. J. Malik, A. Beqiri, A. N. Price, J. N. Teixeira, J. W. Hand, J. V. Hajnal. NMR in Biomedicine Vol. 28 (2015) 344–352, DOI: 10.1002/nbm.3256

[18] *Power balance and loss mechanism analysis in RF transmit coil arrays*. A. Kuehne, S. Goluch, P. Waxmann, F. Seifert, B. Ittermann, E. Moser, E. Laistler. Magnetic Resonance in Medicine (2014), DOI: 10.1002/mrm.25493

[19] *Modular 32-Channel Transceiver Coil Array for Cardiac MRI at 7.0T*. A. Graessl,W. Renz, F. Hezel, M. A. Dieringer, L. Winter, C. Oezerdem, J. Rieger, P. Kellman, D. Santoro, T. D. Lindel, T. Frauenrath, H. Pfeiffer, Th. Niendorf. Magnetic Resonance in Medicine (2014), DOI: 10.1002/mrm.24903

[20] *MR System Operator: Recommended Minimum Requirements for Performing MRI in Human Subjects in a Research Setting.* F. Calamante, W. H. Faulkner Jr., B. Ittermann, E. Kanal, V. Kimbrell, T. Owman, S. B. Reeder, A. M. Sawyer, F. G. Shellock, J. S. van den Brink on behalf of the ISMRM Safety Committee. Journal of Magnetic Resonance Imaging (2015),41, 899-902, DOI: 10.1002/jmri.24717

[21] *Reference dosimetry in the presence of magnetic fields: conditions to validate Monte Carlo simulations*. H. Bouchard, J.A. de Pooter, Alex Bielajew, S. Duane. Physics in Medicine & Biology 60 (2015) 6639. DOI: 10.1088/0031-9155/60/17/6639

[22] *Numerical Prediction of Temperature Elevation Induced Around Metallic Hip Prostheses by Traditional, Split and Uniplanar Gradient Coils*. L. Zilberti, O. Bottauscio, M. Chiampi, J. Hand, H. Sanchez Lopez, R. Brühl, S. Crozier. Magnetic Resonance in Medicine (2015). DOI: 10.1002/mrm.25687

[23] *Metrology to support therapeutic and diagnostic techniques based on electromagnetics and nanomagnetics*. G. Barrera, M. Borsero, O. Bottauscio, F. Celegato, M. Chiampi, M. Cöisson, D. Giordano, M. Inguscio, A. Manzin, E. Simonetto, P. Tiberto, L. Zilberti. Rend. Fis. Acc. Lincei. DOI: 10.1007/s12210-015-0386-5

[24] *Assessment of exposure to MRI motion-induced fields based on the International Commission on Non-Ionizing Radiation Protection (ICNIRP) guidelines*. L. Zilberti, O. Bottauscio, M. Chiampi. Magnetic Resonance in Medicine (2015). DOI: 10.1002/mrm.26031

[25] *It goes to 11: A scalable home-built transmit array beyond eight channels.* A. Kühne, P. Waxmann, W. Hoffmann, H. Pfeiffer, R. Seemann, F. Seifert, O. Speck, B. Ittermann. Proc. ISMRM (2015), 23, 3147.

[26] *Correlation of psSAR and tissue specific temperature for 7T pTx head coils - a large scale simulation study*. F. Seifert, G. Weidemann, B. Ittermann. Proc. ISMRM (2015), 23, 380

[27] *RF current measurements in implanted wires in phantoms by fiber optic current clamps*. G. Weidemann, F. Seifert, W. Hoffmann, B. Ittermann. Proc. ISMRM (2015), 23, 1852

[28] *Two-dimensional shaped voxel MRS in the human brain at 3 T*. P. Waxmann, R. Mekle, F. Schubert, A. Kuehne, T. Lindel, F. Seifert, O. Speck, B. Ittermann. Proc. ISMRM (2015), 23, 421

[29] *A system for in situ S-parameter measurements of MR transmit arrays*. G. Weidemann, F. Seifert, W. Hoffmann, R. Seemann, P. Waxmann, B. Ittermann. Proc. ISMRM (2015), 23, 1775

[30] *A method for the measurement of the RF power radiated by 7T transmit coils*. G. Weidemann, F. Seifert, W. Hoffmann, H. Pfeiffer, B. Ittermann. Proc. ISMRM (2015), 23, 1865

[31] *Q matrix approach to control implant heating by transmit array coils*. F. Seifert, G. Weidemann, B. Ittermann. Proc. ISMRM (2015), 23, 3212

[32] *Metrology for MRI Safety*. B Ittermann, O. Bottauscio, J.W. Hand, J. de Pooter, L. de Prez, H. Rabus, F. Seifert, H. Szymanowski, G. Weidemann, L. Zilberti. Proc. 17th International Congress of Metrology, 09001 (2015), DOI: 10.1051/metrology/20150009001